NTNU

Det skapende universitet

Utvikling av prosedyre for overvåking av nikkel og kobolt i avløpsvann fra metallurgisk industri

Mia Cathrine Hellandsjø Holden

Abstract

The possibility of using differential pulse anodic stripping voltammetry (DPASV) for simultaneous measurements of the nickel(II) and cobalt(II) concentration in waste water from Glencore Nikkelverk nickel refinery has been explored. A polycrystalline gold electrode was used as the working electrode in the experiments. The optimal voltammetric settings and experimental procedure for detection of nickel and cobalt by DPASV in the waste water has been investigated. The relationship between the measured analyte response and the nickel and cobalt concentration in solution was established by generating a standard addition calibration curve. Statistical calculations and inference were used the to check the reproducibility of the DPASV method and to validate the calibration curve.

Control of the pH of the solution in which nickel(II) and cobalt(II) is to be detected was found to be very important. If the pH of the solution is too low the working window of the gold electrode is too restricted by the hydrogen wave in the cathodic direction for nickel and cobalt detection by DPASV to be possible. In solutions of pH ten and above the hydrogen wave was shifted far enough down in to the cathodic potential area for nickel and cobalt detection to be possible.

The simultaneous detection of nickel and cobalt in waste water by DPASV was not possible, due to overlapping peaks, without the use of complexing agents. Glycine was found to be the most effective complexing agent. Because the use of additional chemicals in the analysis was unwanted, work was focused on measurements of the combined nickel and cobalt concentration by DPASV.

The application of a pretreatment procedure to activate and stabilise the gold electrode was also found to be important for the reproducibility of the method. Without regular use of the pretreatment procedure the variations in the measured concentration of nickel and cobalt were so large that statistical inference on the data concluded that the observed variations could not be the result of only random error.

A linear standard addition calibration curve was determined to be appropriate to describe the relationship between the measured response and the concentration of nickel and cobalt in the waste water by statistical calculations. The coefficient of determination, R^2, of the calibration curve was 0.9998.

Sammendrag

Muligheten for å bruke differensialpuls anodisk stripping voltammetri (DPASV) for samtidig bestemmelse av nikkel (II)- og kobolt (II)-konsentrasjonen i avløpsvannet fra Glencore Nikkelverk er blitt undersøkt. En polykrystallinsk gullelektroden ble brukt som arbeidselektrode i eksperimentene. De optimale voltammetriske parametrene og den optimale eksperimentell prosedyren for påvisning av nikkel og kobolt i avløpsvann ved DPASV er blitt bestemt. Forholdet mellom den målte analytten responsen og nikkel- og koboltkonsentrasjonen i avløpsvannet ble etablert ved å generere kalibreringskurve etter standard tilsetning metoden. Statistiske beregninger og statistisk inferens ble brukt for å kontrollere reproduserbarheten av DPASV-metoden, og for å validere kalibreringskurven.

Kontroll av pH-verdien i løsningen som nikkel(II) og kobolt(II) skal detekteres i, ble funnet å være meget viktig. Hvis pH i oppløsningen er for lav vil arbeidsvinduet til gullelektroden være så begrenset av hydrogenbølgen i katodisk retning at nikkel- og kobolt-deteksjon ved DPASV er mulig. I løsninger med pH-verdi ti og høyere er hydrogen bølgen forskjøvet langt nok ned i det katodiske potensialområde slik at nikkel- og kobolt-deteksjon er mulig.

Samtidig deteksjon av nikkel og kobolt i avløpsvann ved DPASV var ikke mulig uten anvendelse av kompleksdannere på grunn av overlappende topper. Glysin ble funnet å være den mest effektive kompleksdanneren. Fordi bruk av ytterligere kjemikalier i analysen av avløpsvannet var uønsket, ble det videre arbeidet fokusert på målinger av den kombinerte nikkel-og koboltkonsentrasjon med DPASV.

En forebehandlingsprosedyre for å aktivere og stabilisere gullelektroden ble også funnet å være viktig for reproduserbarheten av målingene. Uten regelmessig bruk av forbehandlingsprosedyren var variasjonen i den målte konsentrasjon av nikkel og kobolt så store at statistisk inferens på resultatene konkluderte med at den observerte variasjonene ikke kunne være et resultat av bare tilfeldige feil.

En lineær standard tillegg kalibreringskurve ble bestemt til å være hensiktsmessig for å beskrive forholdet mellom den målte analytiske responsen og konsentrasjonen av nikkel og kobolt i avløpsvannet ved statistiske beregninger. Korrelasjonskoeffisienten, R^2, for kalibreringskurven var 0,9998 .

Forord

Denne oppgaven markerer slutten på mine fem år som kjemistudent ved Norges teknisk-naturvitenskapelige universitet. Det har vært fem fine år med mange utfordringer og gleder.

Helt siden jeg gjennomførte der første fagene i analytisk kjemi tidlig i studiet har interessen for dette emnet vært til stede. Jeg er derfor svært takknemlig for at jeg fikk gjennomføre en masteroppgave innenfor dette området, selv om det ikke er en studieretning på min linje. Takk til studieveileder ved Institutt for kjemi Thea Fines Berg som gjorde dette mulig.

Takk til min veileder Øyvind Mikkelsen for upåklagelig humør, uendelig kunnskap, generøsitet og tilrettelegging gjennom hele arbeidet med denne oppgaven.

Takk til Torkild Eivindson og de andre ansatte ved Glencore Nikkelverk i Kristiansand for at jeg fikk gjennomføre denne oppgaven med dere. Deres store interesse for mitt arbeid, samt pågangsmot og positive holdning gjennom hele prosessen har vært høyt verdsatt.

Declaration of compliance

I hereby declare that this is an independent work in compliance with the exam regulations of the Norwegian University of Science and Technology.

<div align="center">

Trondheim, February 2nd, 2013

Mia Cathrine Hellandsjø Holden

</div>

Contents

1 Introduction

During the last decade there has been a growing focus on maintaining and improving the water quality of rivers, lakes and other water sources through continuous monitoring of trace metals and environmental pollutants [1–4]. Among the most common analytical techniques used for environmental monitoring and analyses are atomic absorption spectroscopr (AAS) [5, 6] and inductively coupled plasma-mass spectroscopy (ICP-MS) [7–9]. These methods however are not suitable for automatic remote monitoring, and require that the samples are brought to laboratories to be analysed [9]. This is inconvenient and expensive. Especially if the desire of continuous monitoring of the water quality is to be met, which requires a large amount of samples.

Contrary to AAS and ICP-MS voltammetric techniques allow the possibility to easily construct apparatus for remote monitoring of metals and other water impurities [9]. Voltammetry is an electroanalytical method that exploits the relationship between electrical quantities, and the chemical properties of analyte species [10]. More specifically, voltammetric techniques measure the current generated by the reduction or oxidation of analyte species at the working electrode as a function of applied potential over an electrochemical cell. Voltammetry is a fast and easy to carry out method, that possesses a good sensitivity towards metals [9]. It is possible to construct inexpensive voltammetric equipment, which makes this method especially suitable for automatic and remote monitoring of metals in rivers, waste waters and seawater.

As part of the growing interest of monitoring the quality of natural waters, there has also been an increased interest of monitoring the metals and pollutants in industrial waste water. The aim of this study has been to develop a voltammetric technique that can be used for automatic monitoring of the nickel(II) and cobalt(II) content in the waste water from Glencore Nikkelverk nickel refinery in Kristiansand, Norway.

Historically, the most prevalent voltammetric methods for nickel and cobalt detection in water samples are polarography [11, 12] or cathodic adsorption stripping voltammetry (AdCSV) [13–16]. Cobalt and nickel have earlier been successfully determined in the waste water from Glencore Nikkelverk by AdCSV [16]. The AdCSV method requires a series of chemicals and the long term stability is inadequate due to the deposition of contaminants on to the electrode surface when the applied potential is scanned in the cathodic direction [16]. This study is therefore focused on developing a differential pulse anodic stripping

voltammetry (DPASV) method for detection of nickel and cobalt in the waste water from the nickel refinery, which. Advantages of DPASV is that it reduces the probability of electrode deactivation due to deposited contaminants, because most species are oxidised off when the electrode potential is scanned in the anodic direction.

2 Theory

In this section the concepts of analytical electrochemistry is presented. Firstly, the electrode process and the current response of mass transport controlled and electron transfer controlled electrode reactions are outlined, to give a general picture of the different current responses in potentiometric techniques. Then, the potentiostatic, electrochemical method used in this study, anodic stripping voltammetry, is described. Following this is a description of elcetrochemical masking and the hydrogen evolution reaction. In the subsections procedures for generation of calibration curves, statistical calculations and statistical interference is provided.

2.1 Electrochemistry

Electrochemistry is the study of the interplay between chemistry and electricity by the transference of electrical charges across interfaces and through solutions [10, 17–19]. Electroanalytical methods exploits the relationship between measured electrical quantities, such as current, potential, or charge, and chemical variables, such as concentration and reaction mechanisms.

Electrochemical measurements are performed in an electrochemical cell [18, 20]. The electrochemical cell consists of two conductors (electrodes), each immersed in a charge transporting solution called an electrolyte. The electrodes and electrolyte solutions are externally connected in such a way that direct contact between reactants is avoided and electrical charge is allowed to flow in the cell. Charge is transferred between the electrodes and electrolyte solutions through reduction-oxidation (redox) reactions involving the electroactive species in the electrolyte solutions on the electrode surface [17]. Redox reactions entail electron transfer from one reactant to another. An example of a redox reaction is given in Equation 1 [20].

$$Cu(s) + 2Ag^+(aq) \rightleftharpoons 2Ag(s) + Cu^{2+}(aq) \tag{1}$$

Any redox reaction, like the one above, can be split into two half-reactions [20]. The half-reactions show which species gains electrons, is reduced, and which species loses electrons, is oxidized. Equation 2 and Equation 3 show the reduction and oxidation half-reactions of

the redox reaction described by Equation 1, respectively.

$$2Ag^+(aq) + 2e^- \rightleftharpoons 2Ag(s) \tag{2}$$

$$Cu(s) \rightleftharpoons Cu^{2+}(aq) + 2e^- \tag{3}$$

In an electrochemical cell the reduction half-reaction occurs at one electrode (the cathode) and the oxidation half-reaction on the other electrode (the anode) [18, 20]. The electrons flow through the external connection between the electrodes from the anode to the cathode. The electrical circuit is completed by the charge transfer that happens in the electrolyte solutions and the external connection they may have.

Electroanalytical methods are usually divided into classes according to the electrical quantity they measure [19]. The two main classes of electroanalytical measurements are potentiostatic and potentiometric. Potentiometry is the measurement of the potential established over the electrochemical cell when (close to) zero current is flowing through the cell. Potentiostatic techniques, at the other hand, involve measurement of the current flowing in the electrochemical cell as a function of cell potential.

In potentiostatic methods the applied potential is used to force a redox reaction involving the target analyte to occur [19]. The current response is used to determine the desired property of the analyte, e.g. concentration or reaction mechanism [19]. The current, at a given applied potential, reflects the rate of electron transfer, thus the current increases as the applied potential reaches a potential region where the electron transfer is thermodynamically or kinetically favourable.

The current produced by reduction or oxidation of the analyte species is called the faradaic current [19]. The faradaic current obeys Faraday's law, which states that the reaction of one mole of substance (transfer of one mole of electrons) involves the transfer of 96 487 Coulomb of charge. It is this relationship that can be exploited when the magnitude of the current response is related to the concentration of analyte species. The non-faradaic current is a result of the charging of the electrode surface (double layer) to the applied potential, secondary reactions and impurities in the electrode, solvent or electrolyte. [19,20]. The non-faradaic current contributes to the measured current, thus making the analytical measurements less accurate.

2.2 The electrode process

The process of charge transfer between the electrodes and the electrolyte solution can be quite complicated and takes place in a sequence of steps, which, as a whole, is termed the electrode process [19, 21]. The simplest electrode processes involve three steps:

1. Mass transport of electroactive species to the electrode

2. Electron transfer across the solution-electrode interface

3. Mass transport of the product back to the bulk solution

More complex electrode processes may include, in addition to the three steps above, chemical and surface reactions, like adsorption and phase formation [19, 21]. These additional processes may occur before and after the actual electron transfer [19].

The rate of the electrode process is limited by the slowest step in the sequence [19]. In general the net rate of the electrode process is limited by either, mass transport of reactants or products, (step 1 and 3 above), or electron transfer (step 2 above) [10, 19]. Whether it is the mass transport process or electron transfer that is the rate determining step depends on the system that is investigated [19]. Electrode material, analytes, sample matrix, operating potential, and time scale are all important factors that take part in determine if the electrode process is mass transport limited, or electron transfer limited.

2.2.1 Mass transport controlled reactions

Mass transport to and from the electrode surface occurs by three different mechanisms [19, 20]:

Diffusion: Spontaneous movement of charged and uncharged species from regions of high concentration to regions with low concentration [10, 19, 20]. The driving force of the diffusional movement is the aim of minimizing the concentration gradient.

Migration: The movement of charged particles through a solution under the influence of an electric field [10, 19, 20]. Cations move towards the negative electrode and anions move towards the positive electrode according to their transport number. Movement of analyte species by migration is unwanted and a supporting electrolyte, excess of charged particles, is often added to the sample solution to avoid this [19].

Convection: Mass transport by mechanical means. This includes forced convection, such as stirring of the solution, or rotation of the electrode, and natural convection resulting from temperature or density gradients [10, 19, 20].

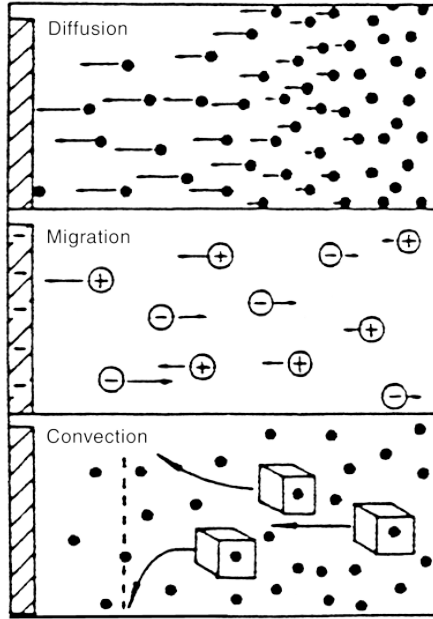The three modes of mass transport is illustrated in Figure 1.

Figure 1: The three mechanisms of mass transport, diffusion, migration and convection [19]

Flux

The rate of mass transport to the electrode, the flux (J), is defined as the number of molecules penetrating a unit area of an imaginary plane in a unit of time [19]. The flux is expressed mathematically by the Nernst-Planck equation, given here for one dimension [19]:

$$J(x,t) = -D\frac{\partial C(x,t)}{\partial x} - \frac{zFDC}{RT}\frac{\partial \phi(x,t)}{\partial x} + C(x,t)V(x,t) \tag{4}$$

where x is distance from the electrode, t is time, D is the diffusion coefficient, $\frac{\partial C(x,t)}{\partial x}$ is the concentration gradient, F is Faraday constant, R is the universal gas constant, T is temperature, $\frac{\partial \phi(x,t)}{\partial x}$ is the potential gradient, z and C are the charge and concentration, respectively, of the electroactive species, and V(x,t) is the hydrodynamic velocity.

The first part on the right side of Equation 4 corresponds to mass transport by diffusion, while the second and third part corresponds to mass transport due to migration and

convection, respectively.

The current (i) is directly proportional to the flux, surface area of the electrode (A), and the number of electron transferred in the redox reaction at the electrode (n) [19]:

$$i = -nFAJ \tag{5}$$

Equation 5 becomes quite complex when all three modes of mass transport occurs simultaneously, thus making it difficult to find a relation between the current and analyte concentration.

Migration of analyte species can be minimized by addition of excess inert electrolyte to the sample solution [19, 20]. The current in the cell is then primarily due to the transport of charged ions in the supporting electrolyte, and the migration term in equation 4 can be neglected, thus simplifying Equation 5.

The Nernst-Plank equation can be further simplified by eliminating mass transport from convection, by using a quiescent solution [19].

In the absence of migration and convection movement of the electroactive species is limited by diffusion [19].

Diffusion controlled current response

Equation 4 without the migration and convection terms yields Equation 6, referred to as Fick's first law [19]:

$$J(x,t) = -D\frac{\partial C(x,t)}{\partial x} \tag{6}$$

Fick's second law describes the rate of change with time of the concentration between parallel planes [19]:

$$\frac{\partial C(x,t)}{\partial t} = D\frac{\partial^2 C(x,t)}{\partial x^2} \tag{7}$$

This equation is valid for linear diffusion between two parallel planes perpendicular to the direction of diffusion, such as a diffusion of analytes towards a planar electrode.

Together Fick's laws describe the flux and the concentration of electroactive species as a function of position and time [10, 19]. Through the use of Laplace transforms and correct boundary conditions a solution of Equation 7 can be found. Together with Equation 6 and Equation 22 the solution of Fick's second law can be used to produce a relationship between the current and analyte concentration, such as the Cottrell equation [19]:

$$i(t) = \frac{nFADC_b}{(\pi Dt)^{1/2}} \tag{8}$$

where C_b is the bulk concentration of analyte species.

This equation holds for any electrochemical method that involves semi-infinite linear diffusion, i.e. diffusion that only occurs perpendicular to the electrode surface, and forms the basis of many electrochemical techniques [18].

During measurements with electrochemical methods, where the mass transport is controlled by semi-infinite linear diffusion, a concentration-time relationship, as the one shown in Figure 2, is established.

As the applied potential reaches the limit where the oxidized form of the analyte species starts to be reduced, the electrode surface concentration quickly approaches zero, and a concentration gradient is established near the surface. As a consequence of this, the region close to the electrode, called the diffusion layer, is depleted of oxidized analyte species. The diffusion layer expands rapidly in the beginning when the concentration gradient is steep, however as the thickness of the diffusion layer (δ) increases the concentration gradient becomes less steep and the expansion of the diffusion layer is slowed down [18, 19].

2.2.2 Electron transfer controlled reactions

As mentioned above, the reaction rate can also be controlled by the rate of electron transfer. The current-potential relationship for reactions where the reaction rate is controlled by the rate of electron transfer is different than the current-potential relationship for diffusion controlled reactions [10, 19]. The effect of the operating potential on the rate of electron transfer can be understood in terms of the activation energy of the electron transfer reaction. The activation energy is a energy barrier towards electron transfer, associated with changes in bond lengths and bond angles that must take place to enable the electron transfer between the oxidized species (O) and the reduced species (R). It is therefore necessary to overcome the activation energy, $\Delta G^{\ddagger}$, for the reaction $O + ne^- \rightleftharpoons R$ to occur. The
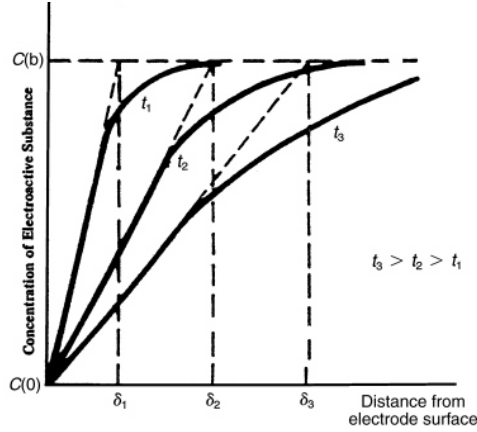
Figure 2: Concentration time gradient at different times after the start of semiinfinite linear diffusion limited electrochemical measurements. The steepness of the concentration gradient decreases with time, as does the diffusion layer thickness (δ). The expansion of the diffusion layer is rapid in the beginning of the experiment, but the rate of expansion decreases as the time increases. [19]

frequency, k, with which an electron is transferred from O to R, and crosses the energy barrier, is given by [19]:

$$k = Ae^{\Delta G^{\ddagger}/RT} \tag{9}$$

where A is a function of the Boltzmann constant, k', and the Planck constant, h, called the frequency factor:

$$A = \frac{k'T}{h} \tag{10}$$

The magnitude of the activation energy is affected by the potential of the working electrode [19]. Changes in the electrode potential alters the energy of the electrons, thus making the reduction reaction more favourable or less favourable. An increase in the activation energy decreases the rate of the reaction and conversely. However, only a fraction (α) of the energy shift is used to change the activation energy. α also reflects the symmetry of the activation energy curve, and it ranges from zero to unity [19].

The new activation energy for the reduction reaction is given by [19]

$$\Delta G_c^\ddagger = \Delta G_{c,0}^\ddagger + \alpha nFE \tag{11}$$

Similarly, the new activation energy of the oxidation reaction [19]

$$\Delta G_a^\ddagger = \Delta G_{a,0}^\ddagger - (1-\alpha)nFE \tag{12}$$

Substitution of Equations 11 and 12 into Equation 9 yields the following equations for reduction [19]

$$k_c = Ae^{-G_{c,0}^\ddagger/RT}e^{-\alpha nFE/RT} \tag{13}$$

and oxidation:

$$k_a = Ae^{-G_{a,0}^\ddagger/RT}e^{(1-\alpha)nFE/RT} \tag{14}$$

The two first factors in Equations 13 and 14 are independent of potential and constants k_c^0 and k_a^0. At equilibrium k_c and k_a are equal so that the two equations can be expresses as follows [19]

$$\underbrace{Ae^{-G_{c,0}^\ddagger/RT}}_{k_c^0}e^{-\alpha nFE/RT} = \underbrace{Ae^{-G_{a,0}^\ddagger/RT}}_{k_a^0}e^{(1-\alpha)nFE/RT} = k^0 \tag{15}$$

Substitution of k_c^0 and k_a^0 from Equation 15 into Equations 14 and 13 gives the relationship between the applied potential and the rate of the reduction and oxidation reactions [19]

$$k_c = k^0 e^{-\alpha nF(E-E^0)/RT} \tag{16}$$

$$k_a = k^0 e^{(1-\alpha)nF(E-E^0)/RT} \tag{17}$$

The reaction rates of the reduction and oxidation reactions depend on the concentration of oxidized and reduced species respectively [19]:

$$r_c = k_c C_O(0, t) \tag{18}$$

$$r_a = k_a C_R(0, t) \tag{19}$$

where $C_R(0, t)$ and $C_O(0, t)$ is the concentration of R and O at the electrode surface respectively.

The rate of the net redox, $r_n et$ reactions [19]

$$r_{net} = k_c C_O(0, t) - k_a C_R(0, t) \tag{20}$$

The cathodic and anodic currents are proportional to r_a and r_c, and the overall current is given as the difference between the cathodic and anodic currents [19]:

$$i_{net} = i_c - i_a = nFA(k_c C_O(0, t) - k_a C_R(0, t)) \tag{21}$$

Substitution the expressions for k_c and k_a into the Butler-Volmer equation yields [19]

$$i_{net} = nFAk^0(C_O(0, t)e^{-\alpha nF(E-E^0)/RT} - C_R(0, t)e^{(1-\alpha)nF(E-E^0)/RT}) \tag{22}$$

This equation describes the current-potential relationship for reactions controlled by the rate of electron transfer.

The exchange current

From Equation 22 it can be seen that at $E = E^0$ there is no net current flowing. However, this does not mean that there is no charge movement [10, 19]. The cathodic and anodic currents are equal in magnitude and run in the opposite direction, thus cancelling each other out. The absolute magnitude of these opposing currents at E^0 is the exchange current (i_0), which is proportional to the standard rate constant:

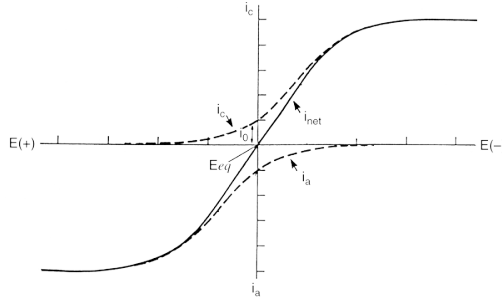$$i_0 = i_c = i_a = nFAk^0 C \tag{23}$$

Figure 3: Figure 3 displays the current-potential relationship for reactions controlled by the rate of electron transfer for the case where $C_o(0,t) = C_R(0,t)$ and $\alpha = 0.5$. The anodic and cathodic current components merges with the net current as the potential becomes increasingly more positive or negative, respectively. The exchange current, i_0, is marked as the magnitude of the cathodic current at the equilibrium potential E_eq [19]

Figure 3 displays the current-potential relationship of reactions controlled by the rate of electron transfer for the case where $C_o(0,t) = C_R(0,t)$ and $\alpha = 0.5$. The cathodic, anodic and net currents are shown. As can be seen from the figure, at E_0 the anodic and cathodic current components are equal in magnitude, corresponding to the exchange current, and the net current is zero. When a large negative potential is applied the cathodic current component increases in magnitude, as a result of the increased charge movement in the cathodic direction, while the anodic current component becomes negligible. The cathodic current component merges with the net current. For the same reasons the anodic current component and net current merge at large positive potentials.

Systems where the magnitude of the exchange current is small are associated with the need for a considerable increase of the applied potential, above the equilibrium value of the redox reaction, E_0, to produce a significant net current [10]. For systems that possess bigger exchange currents only a small deviation from the equilibrium potential produce a significant current.

At large negative overpotentials the second term of the Butler-Volmer equation may be neglected,thus in terms of the exchange current the equation becomes:

$$i_{net} = i_0 \left(e^{-\alpha n F (E - E^0)/RT} \right) \tag{24}$$
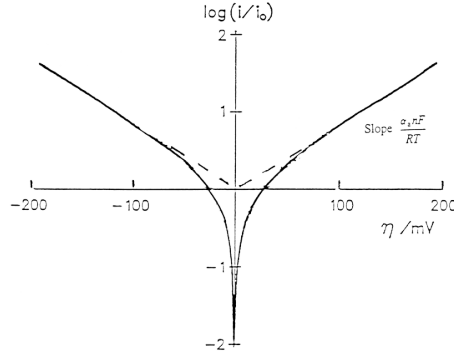
Taking the logarithm on both sides yields:

Figure 4: Tafel plot for the cathodic and anodic current brances of the current-potential relationship curve [19]

$$ln(i_{net}) = ln(i_0) - \alpha nF(E - E^0)/RT \tag{25}$$

Equation 25 can be used to derive information about the kinetically important parameters α and i_0. By plotting $ln(i_0)$ against $E_0 - E$ the Tafel plot is obtained, as show in in Figure 4. Rearranging Equation 25 gives:

$$E_0 - E = a - \frac{2.303RT}{\alpha nF} \tag{26}$$

where values of the slope, $b = \frac{2.303RT}{\alpha nF}$ indicates the rate of the reaction as a function of the applied potential. Often the Tafel plots and Tafel slope is used to decide the mechanisms of the hydrogen evolution reaction (see section 2.5). The extrapolation of the linear part of the plot to zero overvoltage gives an intercept at the exchange current. When the overpotential approaches zero, the current is limited by the mass transport to the electrode because of restrictions imposed by the rate at which the reactants can reach the surface. This is called kinetic polarization and results in a non-linear Tafel slope near the zero overvoltage region.

2.2.3 Polarization effects

For a reversible electrochemical system that follows the laws of thermodynamics the electrode potential is a function of the concentration of electroactive species according to the Nernst equation [19]:

$$E = E^0 - \frac{RT}{nF}ln\frac{C_R(0,t)}{C_O(0,t)} \tag{27}$$

where E^0 is the standard potential for the half-reaction, R is the universal gas constant, T is the temperature, n is the number of electrons being transferred in the reaction, F is the Faraday constant, and $C_R(0,t)$ and $C_O(0,t)$ is the concentration of reduced and oxidized species respectively.

Reversible electrochemical systems also exhibit a linear relationship between the current flowing in the cell and the potential of the cell [19, 20]. Ohm's law describes the current response, I, in a cell as a function of the cell's resistance, R, and potential, E.

$$I = \frac{E}{R} \tag{28}$$

The term polarization refers to the departure of the electrode potential from the theoretical Nernst value when current is passed through a cell [20]. Polarized systems exhibit a non-linear behaviour between the applied potential and current response, as shown in Figure 5. The degree of polarization is given by an overpotential, Π. The overpotential is the potential difference between the actual potential of the cell and the Nernst potential at a given current.

Two types of polarization exists, concentration polarization and kinetic polarization [20].

Concentration polarization occurs when the transport to and from the electrode of reactants and product is too slow to maintain the current predicted by the Nernst equation. This is also evident from the non-linearity of the Tafel plots near zero overvoltage. The exact potential when concentration polarization occurs is dependent on the diffusion coefficient and the agitation of the solution.

Kinetic polarization occurs when the current is limited by the rate of electron transfer between the reactants and the electrodes. This type of polarization is more common among reactions that produce gases.
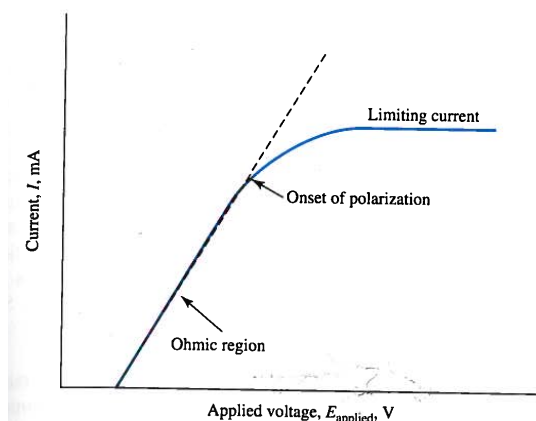
Figure 5: Current-potential curve showing the omic region, and the onset of polarization [20]

2.2.4 The electrical double layer

To compensate for the excess charge on the electrode (q_e), a layer of charged particles and/or oriented dipoles accumulate in the vicinity of the electrode surface [19, 22]. This layer carries a charge (q_s) that is equal and opposite to q_e, since the interface must be neutral. Accordingly, the counterlayer, called the electrical double layer, consists of ions of opposite charge to the electrode.

In the Stern model, the electrical double layer is divides into three separate parts [22]. The *inner Helmholtz plane* (IHP), the *outer Helmholtz plane* (OHP), and the *diffuse layer*.

The inner Helmholtz plane consists of specifically adsorbed ions that are not hydrated [19]. The outer Helmholtz plane consists of non-specifically adsorbed, solvated ions, that are attracted to the surface by long range Coulombic forces. The OHP passes through the center of the solvated ions at their closest approach to the surface. The diffuse layer extends from the OHP to the bulk solution, and consists of scattered ions. Figure 6 displays the division of the electrical double layer (EDL).

Figure 7 shows the potential distribution in the EDL. In the IHL and OHL the potential increases linearly, but in the diffuse layer the potentials increases exponentially [19]. The thickness of the electrical double layer, the expansion into the bulk solution, is affected by the size, valence and concentration of the counter ions [22]. The thickness of the EDL decreases with increasing concentration and valence of the counter ions. The size of the counter ions determine their ability to adsorb to the electrode surface. Larger ions are more polarizable and less hydrated, thus they adsorb more easily to the electrode surface. Such that an increase in size of the counter ions decreases the thickness of the electrical

double layer.

The electrical double layer structure may affect both reaction order and Tafel slopes, which in turn will make reaction mechanism determination uncertain, if the effect of the EDL on the reaction order and Tafel slope are are not accounted for in calculations [23].
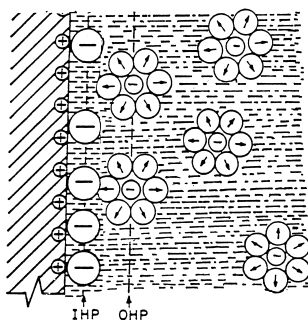
Figure 6: Illustration of the inner Helmoltz plane (IHP), the outer Helmholtz plane (OHP), and the diffuse layer of the electrical double layer. The IHP consists of specifically adsorbed ions, while the OHP consists of solvated, nospecifically adsobed ions. The diffuse layer extends from the OHP to the bulk solution and consists of scattered ions. [19]
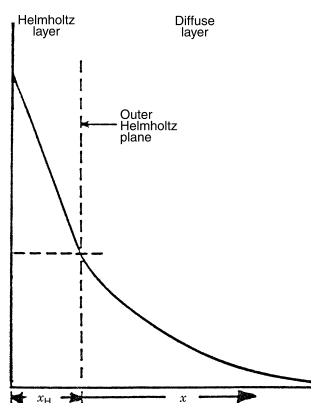
Figure 7: Potential-distance distribution in the electrical double layer surrounding the ellectrode. [19]

2.3 Voltammetry

Voltammetry is a potentiostatic, electrochemical technique that depends on the measurement of current as a function of applied potential [10, 19–21]. As an analytical method voltammetry is widely used for determination of metals and trace metals in the environment, but other inorganic species and organic species can be determined. Voltammetry is

also used for studies of electron transfer mechanisms, adsorption processes on surfaces and redox reactions in various media [10, 19].

The method is both selective and sensitive, and is capable of measuring several spices in a single scan. Other advantages are its low initial, as well as running costs, and the possibility of on-line monitoring due to the compact size and easy to use instrument [9, 20]

During voltammetric measurements the potential that is applied to the electrodes is varied systematically with time [20]. The shape of the applied potential-time function is called the waveform, and different voltammetric techniques are classified by the shape of their waveform. These include linear sweep voltammetry, differential pulse voltammetry, square wave voltammetry and cyclic voltammetry [20]. Voltammetric measurements are often preceded by a bulk electrolysis preconcentration step where the analyte is deposited on the electrode. The deposited analyte is then determined by one of the voltammetric techniques described above. During this step the analyte is stripped of the electrode. Examples of voltammetric stripping techniques are anodic stripping methods, cathodic stripping methods and adsorption stripping methods [20].

2.3.1 Voltammetric instrumentation

Figure 8 shows the components of a typical three electrode system that is used in voltammetric measurements. The system consist of a working electrode, reference electrode, and a counter electrode immersed in a sample solution. The working electrode and the reference electrode are connected in a circuit containing a voltmeter. Because of the high resistance of the voltmeter essentially no current is flowing in this circuit during the measurements. Hence, this circuit is used to measure the potential of the working electrode against the reference electrode during analysis. The working electrode and the counter electrode is connected in another circuit, through which the current is allowed to flow [20].

The aim of the three electrode system is to minimize the ohmic potential of the cell [20, 21]. All the components of the voltammetric cell, including the sample solution, will to some extent resist the flow of charge in the cell [20]. Ohm's law describes the potential drop, E_{Ohm}, associated with this resistance towards charge flow in the cell, R_{cell}, that occurs when a current, I_{cell}, of a given magnitude is flowing in the cell [20]:

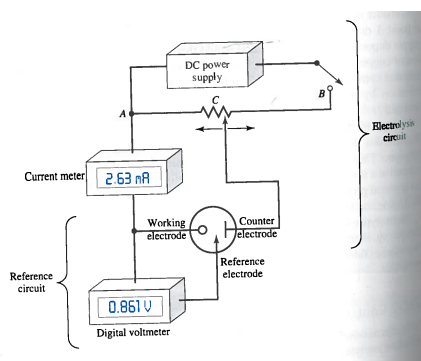$$E_{Ohm} = I_{cel}R_{cell} \qquad (29)$$

Figure 8: Typical voltammetric three electrode system. The voltmeter monitors the potential between the working and reference electrode, while the potential between the working and counter electrode is changes to maintain the desired potential at the working electrode versus the reference electrode. The current flowing in the reference circuit is close to zero. The analytical current is allowed to flow in the electrolysis circuit. [20]

Therefore, to generate a current of a given magnitude in the cell it is necessary to apply a potential that is, E_{Ohm}, more negative than the thermodynamic cell potential given by the Nernst equation [20]. Thus, the potential of the working electrode will drift towards a more negative potential as current passes through the cell.

With the three electrode arrangement only a very small current passes between the working electrode and the reference electrode, which minimizes the ohmic potential and makes it possible to keep the working electrode at a constant, desired potential [20].

Concentration polarization and kinetic polarization also contribute to ohmic potential and potential drift of the working electrode. This is also overcome by the three electrode system.

2.3.2 Stripping analysis at solid electrodes

Stripping analysis is a sensitive voltammetric technique well suited for the determination of trace metals [19]. In stripping methods the analyte is initially deposited on the surface of the electrode in a bulk electrolysis step. Following the preconcentration step the accumulated analyte is stripped of by a voltammetric procedure [20]. Different stripping methods can be applied, differing in the nature of the preconcentration and stripping step [19]. It is the combination of the preconcentration step and advanced stripping methods which enables the high sensitivity of the method [19].

Anodic stripping voltammetry

In anodic stripping voltammetry (ASV) the species of interest are preconcentrated on to the electrode surface by applying a cathodic potential to the electrode [19, 24]. The deposition time is determined by the concentration of species in solution, and increases as the concentration of species in solution increases. The deposition potential is generally set to be 0.3-0.5 V lower than the E^0 of the least reducible species to be determined [19]. Convective transport of reducible species to the electrode surface is ensured by rotating the working electrode or stirring the solution.

Subsequently the deposited species are stripped off by scanning the potential in the anodic direction, often by using a differential pulse waveform [19, 24]. The different species are oxidized off according to their standard potential, producing an oxidation current that is used to detect the species.

The kinetics of the deposition of metals on the electrode is highly dependent on the composition of the supporting electrolyte and on the type of the electrode pretreatment [25]. The peak potential and the sensitivity of the electrode towards the metals changes as the electrolyte and pretreatment are changed [25–27]. The structure of the electrode-electrolyte interface also plays an important part in determining deposition kinetics [28].

Disturbances include, inability to distinguish two or more species due to similar oxidation potentials. Surface active substances that block the surface and the formation of intermetallic substances during deposition [24, 29].

Subtractive Anodic Stripping Voltammetry

Subtractive anodic stripping voltammetry (SASV) [25–27, 30] is a technique that allows analysis at very low analyte concentrations by removal of interferences from the sample matrix including the presence of oxygen. This is achieved by subtracting a background voltammogram, recorded using zero deposition time, from the regular stripping voltammogram. The two voltammograms are recorded immidiately after one another to minimize the differences in experimental conditions. SASV can increase peak separation and the detection limit of a voltammetric method [25–27, 30]. The SASV method is especially suitable when the stripping peaks are asymmetric, the background around the peaks of interest varies, and when the sample solutions is very diluted such that small variations in electrode surface and sample matrix throughout the analysis affect the reproducibility.

2.3.3 Electrode materials

The choice of working electrode material is very important in voltammetric analyses, as it determines the species that can be detected and measured [19, 31]. The electrode material also decides the width of the potential window, the degree of interference, additional chemicals needed and maintenance. Other important working electrode properties include high signal to noise ratio, high electrical conductivity, surface reproducibility and high sensitivity towards several analytes. In addition, the electrode material should be easy to manufacture, be chemically stable and give reproducible response.

The gold electrode

Gold is one of the most common noble metal electrodes used for stripping measurements [24]. The gold electrode exhibits a lower overpotential towards HER than mercury, however, it is less easily oxidized. This limits the ability of the gold electrode to detect species with highly negative redox potentials. In addition the adsorption of hydrogen decreases the sensitivity of the electrode, thus the deposition potential should be selected carefully to avoid unnecessary loss of sensitivity [24]. Stripping analysis at metallic electrodes can be complicated by alteration of the electrode kinetics due to oxide film formation on the electrode surface when the electrode is scanned at anodic potentials [24]. Thus, the anodic working window of the gold electrode is limited to +0.7 V if build up of oxide film is to be avoided [24].

Activation and cleaning of the gold electrode

Activation or pretreatment has been reported to be essential for reproducibility and stability of the gold electrode in anodic stripping analysis. Freshly polished gold electrodes display ill-defined voltammograms in detection of different metals in different solutions [25–27]. Evolving oxygen at the electrode surface, which results in oxide layer formation, has been reported as a method to activate the gold electrode [25]. Several consecutive anodic stripping voltammetry runs has also been reported to improve the stability of the electrode [25].

The determination of metals at a gold electrode can be negatively affected by the incomplete removal of deposited metal from previous scans [32]. To eliminate the build up of deposited metal, and increase the reproducibility of subsequent analyses, electrochemical and a mechanical cleaning procedure are essential. The electrode surface can be electrochemically cleaned by applying a anodic potential to the electrode for a short amount of

time while the electrode is kept in an electrolyte solution [33]. The choice of electrolyte may influence the effectiveness of the electrochemical cleaning procedure [32]. The cleaning and activation procedure can be repeated after every scan or when the performance of the electrode deteriorates [25, 32]. Whenever the electrochemical cleaning is no longer effective mechanical cleaning can be applied [25–27, 32]

2.4 Electroanalytical masking and complex formation

Complexes can be formed between metal ions and electron pair donor species called ligands [20]. The ligand's electron pair is used to form a covalent bond between the metal ion and the ligand. The number of ligands that is covalently bonded to the metal ion is referred to as the coordination number of the metal. The number of ligands coordinated to a metal ion is a result of the structure and electron configuration of the ligand and metal ion.

The formation of a complex, ML, takes place in several steps [20]. Each step involves the additions of a ligand, L, to the metal ion, M:

$$M + L \rightleftharpoons ML \qquad K_1 = \frac{[ML]}{[M][L]} \tag{30}$$

$$ML + L \rightleftharpoons ML_2 \qquad K_2 = \frac{[ML_2]}{[ML][L]} \tag{31}$$

$$ML_2 + L \rightleftharpoons ML_3 \qquad K_3 = \frac{[ML_3]}{[ML_2][L]} \tag{32}$$
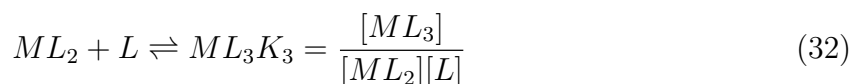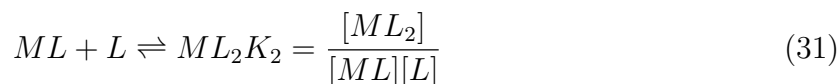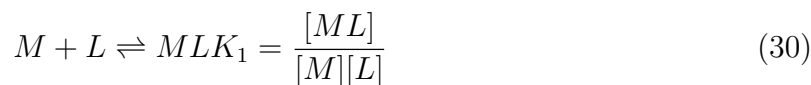
The overall formation constant of the complex, K, is the product of each of the stepwise formation constants, K_1, K_2 and K_3.

Electroanalytical masking

The simultaneous quantitative determination of metals with voltammetric techniques relies on an adequate separation between the successive peak potentials of the metals [34]. The minimum separation in peak potential that is necessary for adequate quantitative determination increases as the difference in relative concentration of the metals in the sample increases. Complex formation can be used to increase the separation of successive peak potential [34]. If the complex formation-dissociation equilibrium is established rapidly, the peak potential is usually displaced to more a more negative potential. The amount of

the displacement is dependent on the stability constant of the complex [34]. Therefore, when two metal ions form complexes with the same ligand, it is the difference in stability constants that will determine the extent of further separation of the peak potentials. The stability constants are ordinarily pH dependant, however this is not always the case. Differences in pH dependence can be exploited to obtain maximum separation of peak potentials by carefully buffering the solution. *Complex formation can also be used to completely mask one or more of the unwanted metal ions because the become electrochemically inactive in the desired potential region.*
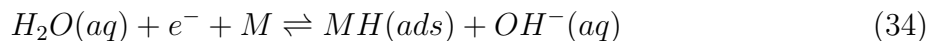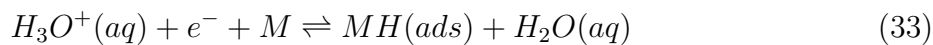
Some of the most common ligands for complex formation with metal ions include, EDTA, carboxylic acids, amines, halides and acetylacetone [34]. Nickel(II) and cobalt(II) are known to form complexes with EDTA, NH_3, citric acid, KSCN and glycine [34,35]. Glycine is known to shift the peak potential of cobalt(II) to more negative potentials at pH between 8.5 and 10 in polarography [35].
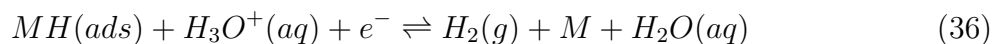
2.5 The hydrogen evolution reaction

The electrochemical evolution of hydrogen gas at the electrode surface is a well known and studied electrochemical phenomenon [10, 21, 36–39]. The hydrogen evolution reaction (HER) occurs at varying negative electrode potentials, depending on the electrode material, sample matrix composition, double layer structure, and adsorption energy of hydrogen at the electrode surface [21]. The potential at which hydrogen gas is formed, for a given electrode, is called the hydrogen overpotential of the electrode. The hydrogen overpotential is considered the end-point of the cathodic potential window, and is therefore an important analytical property of the electrode, as it limits the working area of the electrode [19]. The limitation is a result of the current associated with the hydrogen evolution reaction rapidly becoming significantly larger than the analytic current, thus making the detection of analytes with reduction potentials more negative than the hydrogen overpotential impossible.

Although the exact mechanism and rate determining step of the HER is debated, three reactions have been identified to participate in hydrogen evolution in two steps [10,21].

The first step in the hydrogen evolution reaction involves the reduction of a proton donor, primarily oxonium ions or water, as shown in Equation 33 and Equation 34, respectively [10, 21, 39]. This process is often called the Volmer reaction.

$$H_3O^+(aq) + e^- + M \rightleftharpoons MH(ads) + H_2O(aq) \tag{33}$$

$$H_2O(aq) + e^- + M \rightleftharpoons MH(ads) + OH^-(aq) \tag{34}$$

In the second step the adsorbed hydrogen is removed from the electrode as hydrogen gas. Two different mechanisms have been proposed for the removal step, the Tafel reaction as shown in Equation 35 and the Heyrovskỳ reaction shown in Equation 36 [21].

$$2H(ads) \rightleftharpoons H_2(g) \tag{35}$$

$$MH(ads) + H_3O^+(aq) + e^- \rightleftharpoons H_2(g) + M + H_2O(aq) \tag{36}$$

2.5.1 Solvent effect on hydrogen overpotential

The rate of hydrogen adsorption has been found to be directly proportional to the concentration of protons in the solution [40–42]. Thus, for hydrogen evolution reactions controlled by the rate of proton reduction the rate of hydrogen gas formation will increase with an decrease in solution pH.

Specific adsorption of anions in the electrical double layer is possible even on negatively charged surfaces [43]. The potential at which the anions are desorbed varies with the electrode and the specific anion of interest [44, 45] The specific adsorption of halide ions increases the overpotential towards hydrogen gas evolution at both the mercury and platinum electrode [42, 45]. The presence of nitrate has no significant impact on the overpotential towards HER of the platinum electrodes [44]. The general trend is that the hydrogen overpotential increases with the ability of the anions to adsorb on the electrode surface and increasing concentration of anions in solution.

2.6   Statistical calculations and inference

In this section the statistical methods used in this study are presented.

2.6.1 Linear calibration

If an analytical method is to be used for quantitative determination it is necessary to know the relationship between the signal that is measured and the analyte concentration in the test solution [46]. This is often achieved by constructing a calibration curve that relates the measured analyte signal to the known analyte concentration in a set of standard solutions [19,46,47]. An unknown sample is then analysed in the same way as the standard solutions and the analyte concentration can be estimated by using the calibration curve. Calibration curves can be linear, curved or both [47]

2.6.2 The least squares method

The calibration curves used in this study are all linear and have been generated using the computer software Microsoft Excel. The computer software uses the least squares method to create the best fitted linear curve through the points generated by the standard solutions. The least squares method is based on four assumptions [20, 47]:

1. There exists a linear relationship between the measured response and the analyte concentration

2. All the errors occur in the signal measurements. When compared, the errors in the concentration of the standard solutions is negligible.

3. The instrument measurement errors are normally distributed

4. The variation in the instrument measurement errors is independent of standard solution concentration

A linear calibration curve calculated by the least squares method has the general formula $y_i = mx_i + b$, where y_i is the measured signal for a given analyte concentration, x_i, and m and b are the slope and intercept of the line, respectively [20, 47, 48]. The best line is calculated by minimizing the sum of the squared distances in the y-direction between the line and the data points, SS_{resid}. The distances are called residuals. SS_{resid} is given by:

$$SS_{resid} = \sum_{i=1}^{N} \{y_i - (b + mx_i)\}^2 \tag{37}$$

Where N is the number of calibration points used.

Three other sum of squares can also be defined. The sum of the squared deviations between each data point, x_i and the mean, $\bar{x}$, SS_{xx}. The sum of the squared deviations between each data point, y_i and the mean, $\bar{y}$, SS_{yy}. The sum of the distances in both x- and y-direction, SS_{xy}. The formulas are shown below.

$$SS_{xx} = \sum (x_i - \bar{x})^2 \tag{38}$$

$$SS_{yy} = \sum (y_i - \bar{y})^2 \tag{39}$$

$$SS_{xy} = \sum (x_i - \bar{x})(y_i - \bar{y}) \tag{40}$$

where $\bar{x}$ and $\bar{y}$ are the means of the analyte concentrations and the measured response, respectively, as given below in Equation 2.6.2

$$\bar{x} = \frac{\sum_{i=1}^{N} x_i}{N} \tag{41}$$

From SS_{xx}, SS_{yy}, SS_{xy} the slope and intercept of the calibration curve can be calculated:

$$m = \frac{SS_{xy}}{S_{xx}} \tag{42}$$

$$b = \bar{y} - m\bar{x} \tag{43}$$

Prediction and errors

The concentration of the unknown sample can now be calculated by using the calibration equation. The predicted analyte concentration is subject to error due to the errors in the calibration equation and the random error in the measured y-values.

The standard deviation of the residuals, also called standard deviation about regression, is the deviation between the y-values and the y-values predicted by the calibration equation, $\hat{y}$ predicted is given as follows:

$$s_r = \sqrt{\frac{\sum\limits_{i=1}^{N} (y_i - \hat{y}_i)^2}{N - 2}} \tag{44}$$

where N-2 is the degrees of freedom, equal to the number of calibration solutions, N, minus the number of parameters fit, in this case slope and intercept.

The standard deviation of the residuals is used to calculate the standard deviation of the slope, s_m, the the standard deviation of the intercept, s_b, and the standard deviation, s_c of the predicted concentration, x_c, obtained from the calibration curve, as shown below:

$$s_m = \sqrt{\frac{s_r^2}{SS_{xx}}} \tag{45}$$

$$s_b = s_r \sqrt{\frac{\sum x_i^2}{N \sum x_i^2 - (\sum x_i)^2}} \tag{46}$$

$$s_c = \frac{s_r}{m} \sqrt{\frac{1}{M} + \frac{1}{N} + \frac{(\bar{y}_c - \bar{y})^2}{m^2 SS_{xx}}} \tag{47}$$

where y_c is the measured signal of a sample solution, M is the number of measurement repetitions of the test solution, and $\bar{y}_c$ is the mean of the measured signals.

Significance of the regression

The total variation in the observed values of y is given by SS_{yy} as described above in Equation 2.6.2 [20]. The sum of the squares of the residuals, SS_{resid}, measures the variation in the y-values that are not explained by the linear model of x and y:

$$SS_{resid} = \sum\limits_{i=1}^{N} \{y_i - (b - mx_i)\}^2 \tag{48}$$

Although generally considered not appropriate [4, 47], the coefficient of determination, R^2, is used as a measure of the quality of the least squares line fitting by Excel. The closer

R^2 value is to unity the better the fit of the line to the data [47]. The coefficient of determination is given by:

$$R^2 = 1 - \frac{SS_{resid}}{SS_{yy}} \tag{49}$$

As an alternative a residual plot can be used to determine if the linear calibration curve is appropriate. A residual plot is a plot of the y-residuals, $\hat{\epsilon}$, with the corresponding x-values. The residuals should lie on a straight line around zero [47]. This often referred to as homoscedasticity [48].

The F test

The difference between SS_{yy} and SS_{resid}, SS_{regr} is a measure of the variation explained by the calibration curve. The number of degrees of freedom associated with each sum of squares depend on the number of parameters that has been estimated to calculate that sum of squares [20, 47]. Thus, SS_{yy} has N-1 degrees of freedom, SS_{resid} has N-2 degrees of freedom, and SS_{regr} has 1 degree of freedom. Based on this, the F value can be calculated

$$F = \frac{SS_{regr}/df_{regr}}{SS_{resid}/df_{resid}} \tag{50}$$

where df_{regr} and df_{resid} are the degrees of freedom of SS_{regr} and SS_{resid}, respectively.

The F value is a measure of the significance of the regression [20]. A significant regression is one where the variation in the y values due to the presumed linear relationship is large compared to the residuals, i.e. the numerator of F is large compared to the denominator, and the F value itself is large. The calculated F value should be compared to a critical F value from a table at a given confidence level. If the calculated F value is larger than the critical F value for the given confidence level, the regression is significant. The confidence level represents the probability of accepting that the regression is significant, when in reality it is not.

Method of standard addition

The method of standard addition is a calibration method that takes into account matrix effects on the measured signal [20, 47]. The samples solution is analysed before known

amounts of the analyte is successively added to the sample solution, and the analyte signal is recorded for each addition. Alternatively, the sample is divided into several parts and known amounts of the analyte is added to all parts but one [46]. For voltammetric measurements the analyte signal is commonly peak height or peak area [19]. The calibration curve is constructed by plotting the recorded signal as a function of the amount of added analyte. The concentration of the sample, x_c is found as the interception between the curve and the x-axis, or numerically:

$$x_c = b/m \tag{51}$$

To find x_c the value of y is set to zero, resulting in that the error in the value of x_c derives only from the errors in the calibration curve itself [47]. Thus, the standard deviation, s_{x_c} of x_c is given by:

$$s_c = \frac{S_r}{m}\sqrt{\frac{1}{N} + \frac{\bar{y}^2}{m^2 SS_{xx}}} \tag{52}$$

Disadvantages of the standard addition method is that a larger amount of sample is needed if the sample is to be divided, and in addition, that strictly each calibration is valid for only one sample [47].

Analytical sensitivity   Calibration sensitivity is defined as the change in signal response per unit change in analyte concentration [20], thus it is the slope of the calibration curve. Analytical sensitivity is the calibration sensitivity divided by the standard deviation of the analytical signal for a given analyte concentration.

Linear dynamic range   The linear dynamic range of an analytical method is the concentration where a linear calibration curve can be used to determine the relationship between analytical response and analyte concentration. Deviation from linearity at high concentrations may be caused by non-ideal detector response or chemical effects [20].

2.7 Comparison of two experimental means by hypothesis testing

In experimental studies information about a population is often inferred from observations made on a subset of the population, for example, the determination of heavy metals in a lake [20]. Small samples of water from the lake are analysed and used to determine the heavy metal concentration in the whole of the lake, the population. The experimental mean of the set approaches the population mean as the number of analysis repetitions increase. Hypothesis testing can be used to determine if the difference in experimental means of two sets is real or the result of random error. If the difference is due to random error the samples come from the same population.

In a hypothesis test a null hypothesis, which assumes that the two means are the same, is accepted or rejected based on the probability that the observed difference in the means is a result of random error or not [20]. The probability distribution of the population is used to calculate this probability [20, 49]. If the observed difference is greater than the difference that would occur by random chance at a certain intensity, the significance level, the null hypothesis is rejected. A significance level of 0.05 yields a 5 % chance of rejecting the null hypothesis when it is true.

The first step of the hypothesis test is to state the the null hypothesis, H_0 and and the alternative hypothesis, H_a.

$H_0 : \mu_1 = \mu_2 0$

$H_a : \mu_1 \neq \mu_2 0$

Secondly, an appropriate test statistic should be formed, based on the probability distribution of the population and the known parameters of this probability distribution [20, 49]. The test statistic is used to decide if the null hypothesis should be rejected or accepted [49]. For a population that is normally distributed, but the variance is unknown, the t statistic, t, is the appropriate test statistic for the hypothesis test on the experimental means of two data sets.

$$t = \frac{\bar{x}_1 - \bar{x}_2}{s_{pooled}\sqrt{\frac{N_1 + N_2}{N_1 N_2}}} \tag{53}$$

where s_{pooled} is given by:

$$s_{pooled} = \sqrt{\frac{\sum\limits_{i=1}^{N_1}(x_i - \bar{x_1})^2 + \sum\limits_{j=1}^{N_2}(x_j - \bar{x_2})^2}{N_1 + N_2 - N_I}} \tag{54}$$

where N_1 and N_2 is the number of replicate results in set 1 and 2, respectively, x_i represents the individual results in set 1, x_j represents the individual results in set 2, $\bar{x_1}$ is the experimental mean of set 1, $\bar{x_2}$ is the experimental mean of set 2, and N_I is the number of pooled data sets.

The pooled standard deviation is a better estimate of the populations standard deviation than the the individual set standard deviations alone. The pooling of the standard deviations can only be done if the individual standard deviations are similar.

The test statistic t has a t distribution with $N_1 + N_2 - N_I$ degrees of freedom. The t statistic is compared to a table t value for the correct number of degrees of freedom, and confidence level. If the calculated t statistic is smaller than the critical t value or larger than the negative critical t value the null hypothesis is accepted.

Errors in hypothesis testing

Type I errors occur when the null hypothesis is rejected when it is true. Type II errors occur when the null hypothesis is accepted when it is false. The probability of type I error is given by the significance level, α. Decreasing the type I error increases the rate of type II error. No test procedure can guarantee that no errors will be committed, and it is important to choose the significance level that is appropriate for the given problem.

P-value

The P-value is the probability that the test statistic will take on a value that is at least as extreme as the calculated value when the null hypothesis is true. The P-value is thus the smallest level of significance that would lead to rejection of the null hypothesis. The P value was found using the *TDIST* function integrated in the Excel software.

3   Experimental

The overall goal of this theses has been to develop an automated voltammteric procedure for simultaneous detection of cobalt and nickel in the waste water from Glencore Nikkelverk nickel refinery. In this chapter the experimental work that has been done, including parameters, equipment and chemicals, that have been used, is presented.

The working electrode, auxiliary electrode and counter electrode used in this study was together with the research and development group at Glencore Nikkelverk chosen to be the same as the electrodes used in already existing voltammetric equipment at the nickel refinery.

Experimental work began by trying to develop a voltammetric method for detection of nickel and cobalt in synthetic solutions. The synthetic solutions consisted of different supporting electrolytes added nickel and cobalt standard solutions. When nickel and cobalt were successful measured in synthetic solution experimental work on the waste water samples from the nickel production plant commenced. As a result of this division in the experimental work it has been natural to divide this chapter in two corresponding sections. One section dealing with the experimental work in synthetic solutions, and one section that addresses the work done in waste water solutions. In addition, a section concerning the experimental equipment, the voltammetric procedure, and chemicals that have been used is included, since these are mostly equal for work in both synthetic and real sample solutions.

Presented first is the section about experimental equipment and chemicals, followed by the section on experimental work in synthetic solutions, and lastly work on the waste water solutions is given.

3.1   Experimental equipment, voltammetric procedures and chemicals

In this section the experimental equipment, the voltammetric procedure, and chemicals that have been used in this study is presented.

3.1.1 Experimental equipment

All analyses was performed with a three electrode system, consisting of a platinum-wire counter electrode and a Ag/AgCl/KCl(saturated) reference electrode. On request from the research and development department at the nickel refinery a polycrystalline, solid gold electrode was used as the working electrode. The gold in the working electrode was encased in a protecting polymer/plastic. The diameter of the working electrodes was 2 mm.

The voltammetric scans were recorded using PalmSens equipment, Software Version 1.3, connected through USB to a computer for parameter setting and data processing.

The cell consisted of a tubular plexiglas container of approximately 50 mL and a plexiglas lid fitted with holes for the electrodes. The electrodes were connected to the PalmSens equipment by wires and clips. A magnetic stirrer was used to for stirring the solution.

Polishing equipment Prior to the very first analysis, the gold electrode was sanded with a coarse paper (P2500) from Buehler to remove a discoloured coating that had occurred during storage. Following this, the electrode was polished to a shiny surface with Nerliens Metaserv 2000 Grinder/Polisher polishing equipment, using a fine grade silicon carbide polishing paper (P4000) from Struers, and rinsed in distilled water. The polishing of the electrode was repeated whenever the electrode was passivated or the sensitivity was significantly deteriorated and electrochemical cleaning was insufficient.

Measuring equipment Volumetric measurements of chemicals were performed using a glass pipettes and measuring cylinders. Dilution of chemical solutions were done in volumetric flasks of glass. Small volumetric measurements were performed using micro-pipettes with sterile tips. Weight measurements were performed on a Precisa XT 1220M scale.

3.1.2 The Differential Pulse Anodic Stripping Voltammetry Procedure

All voltammetric scans in this study were performed using differential pulse anodic stripping voltammetry (DPASV). Deposition potentials ranging from -1.5 V to -0.9 V were applied to pre-concentrate nickel and cobalt on to the working electrode. Deposition times varied from 30 seconds to 600 seconds, depending on the concentration of metals in the sample. The samples solution was stirred throughout the deposition step at approximately 1000 rpm. Between deposition and stripping the working electrode was equilibrated at 0 V

for 10 seconds in a still solution. During the stripping step a differential pulse voltage-time function (waveform) was applied to the working electrodes, as displayed in Figure 9. The scan rate, voltage step, pulse amplitude and pulse time used during the stripping scan typically were 15 mV/s, 5 mV, 50 mV, and 50 ms, respectively. However other parameters were tested. A still electrode was used during this step. One scan usually ranged from -0.9 V to 0.4 V. An overview of the range of DPASV experimental settings that have been used is given in Table 1

The parameters presented here are general. Where appropriate, further specifications of the DPASV parameters that have been used to obtain a particular scans or results presented in Section 4 will be given there.
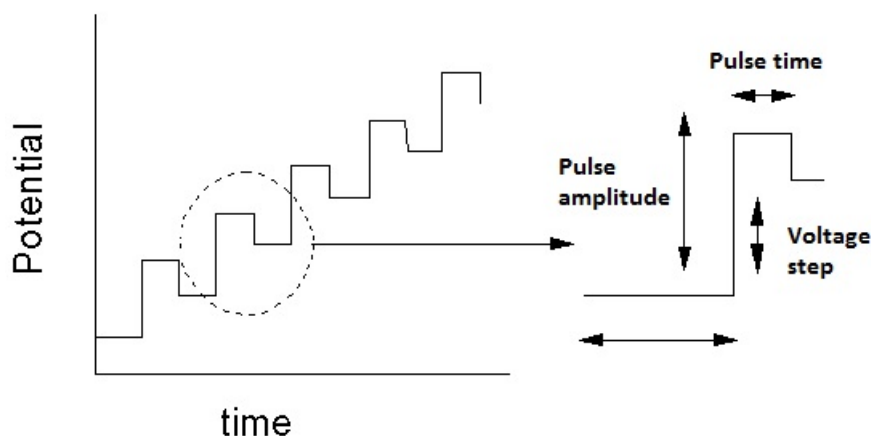

Figure 9: The voltage-time function (waveform) that was applied to the working electrodes during the stripping step of the DPASV procedure.

3.1.3 Chemicals

The chemicals that have been used in this study can mainly be divided into three categories: electrolytes, complexing agents, and metal standards. Below, Table 2, Table 3, and Table 4 list the electrolytes, complexing agents, and metal standards that have been used, respectively.

The chemicals in Table 2 were used to make different electrolytes that offered pH control and improved nickel and cobalt detection.

Saturated potassium chloride solution was used to replenish the reference electrode. In addition, the three electrodes were stored in ammonium chloride solution or water when not in use.

Table 1: DPASV settings

Parameter	Value
Scan rate	10 mV/s - 20 mV/s
Voltage step	5 mV
Pulse voltage	50 mV
Pulse time	50 ms
Deposition potential	-1.5 V to -0.8 V
Deposition time	30 s to 600 s
Stirring	1000 rpm
Start potential	-1.0 V to -0.7 V
Stop potential	0.4 V to 1.0 V
Equilibrium potential	0 V
Equilibrium time	10 s
Activation potential	0.9 V
Activation time	10 s to 50 s

The complexing agents were used to improve the separation of the nickel and cobalt in the analyses.

The metal standards were used to make synthetic nickel and cobalt sample solutions and for internal standard addition.

Table 2: Matrix Chemicals

Name	Formula	Grade	Manufacturer	Note
Ammonia	NH_3	AnalaR Normapur.	VWR	25 % by weight
Potassium chloride	KCl	Pure	Metrohm	
Ammonium chloride	NH_4Cl	P.A.	Sigma-Aldrich	
Nitric acid	HNO_3	P.A.	Merck	65 % by weight
Water	H_2O	Pure	Millipore	

3.2   Synthetic solutions

Initially, experimental work was performed in synthetic solutions consisting of different electrolytes added a nickel standard solution. For each solution, after polishing the working electrode a stable baselines was obtained by performing several differential pule scans from the potential at which the hydrogen wave began to 0.4 V. Thereafter, the DPASV parameters were varied within the range given in Table 1 to try and detect nickel. Electrolytes

Table 3: Complexing Agents

Name	Formula
Disodium ethylenediaminetetraacetic acid	$C_10H_16N_2O_8Na_2$
Citric acid	$C_6H_8O_7$
Potassium thiocyanate	KSCN
Glycine	$C_2H_5NO_2$
Ammonia	NH_3

Table 4: Metal Standards

Name	Description	Manufacturer
Nickel	1000 mg/L in 2.5 % HNO_3	Teknolab A/S
Cobalt	1000 mg/L in 2.5 HNO_3 %	Teknolab A/S

that were tested include, dilute hydrochloric acid (pH 3), nitric acid (pH 2), phosphate buffer (0.01 M, pH 8), ammonium buffer (0.01 M, pH 10), and ammonium chloride solution (0.01 M).

When the optimal electrolyte solution was identified, work then continued to find the optimal experimental settings for the detection of nickel.

The external standard calibration method was applied by analysing sample solutions that varied in nickel concentration from 25 mg/L to 100 mg/L, to check the linear range of the DPASV method. The same procedure was repeated for detection of cobalt. The significance of the external calibration curves was validated by statistical calculations.

Simultaneous detection of nickel and cobalt in synthetic solution When both nickel and cobalt had been successfully detected separately, simultaneous detection of nickel and cobalt was attempted. The same concentrations of nickel an cobalt as used in the measurement of the single metals were used. The deposition time and potential was set to that of cobalt since cobalt needed a more negative deposition potential and longer deposition time than nickel at the same concentration. The higher sensitivity towards nickel resulted in a total merging of the cobalt and nickel peaks. Work began on finding a complexing agent that could separate the two peaks.

3.2.1 Complexing agents

To try and separate the two peaks different complexing agents were tested. In Table 3 all the different complexing agents that were tested and their concentration in the sample are shown.

Table 5: Complexing Agents

Name	Formula	Concentration in ammonia buffer
Na$_2$EDTA	C$_1$0H$_1$6N$_2$O$_8$Na$_2$	1 μM - 7 μM
Citric acid	C$_6$H$_8$O$_7$	0.7 μM - 3.3 μM
Potassium thiocyanate	KSCN	1.7 μM - 20 μM
Glycine	C$_2$H$_5$NO$_2$	2 μM - 29 μM
Ammonia	NH$_3$	mmol/L - mmol/L

3.3 Nickel and cobalt measurements in waste water from the nickel refinery

Normally, the cobalt concentration in the waste water from the nickel refinery is insignificant compared to the nickel content. Therefore, it was decided due to the trouble of separating the two metal peaks, to measure the total amount of cobalt and nickel as one peak. Several different samples of waste water from Glencore Nikkelverk were provided. See Appendix C for details about the waste water samples.

The waste water samples were diluted with ammonium buffer (0.01 M, pH 10) before analysis by DPASV to minimize matrix effects due to a variable matrix composition of the waste water.

Optimization of the experimental settings, dilution ratio and pretreatment procedure for detection of nickel and cobalt in waste water was carried out. A two mean hypothesis test was used to validate the reproducibility of the results.

A standard addition calibration curve for the detection of nickel by differential pulse anodic stripping voltammetry in a waste water sample from the nickel refinery was generated. 100 μL nickel-standard (30 $\mu L/g$) was added to the waste water sample and analysed by differential pulse anodic stripping voltammetry. This was repeated three times. The significance of the standard addition calibration curves was validated by statistical calculations.

4 Results and Discussion

The aim of this study has been to develop and test a voltammetric procedure for the determination of nickel(II) and cobalt(II) in the waste water from Glencore Nikkelverk nickel refinery in Kristiansand, Norway. In this section the results of the study are presented together with a discussion of the findings.

Experimental work began by development of a voltammetric procedure for nickel(II) and cobalt(II) detection in synthetic solutions, before the work on the nickel refinery waste water began. This section follows the same division. Firstly, the results, and discussion of the results, from the experimental work in synthetic solutions is presented in the section *Nickel and cobalt detection in synthetic solutions*. Before the results, and the discussion of the results, from the experimental work on the waste water is presented in section *Nickel and cobalt detection in nickel refinery waste water*.

4.1 Nickel and cobalt detection in synthetic solutions

As described in section 3 experimental work began by searching for an electrolyte that would allow the detection of nickel and cobalt with the gold electrode. Nitric acid solution, phosphate buffer, and ammonium chloride solution were tested. However, the working window of the gold electrode was restricted in the cathodic direction by the hydrogen wave to such a degree in all the above mentioned solutions, that any peaks due to the presence of nickel were hidden regardless of the voltammetric settings. To shift the hydrogen wave to a more negative potential, and at the same time have some pH control, an ammonia buffer solution was then tested as supporting electrolyte. In ammonia buffer (0.01 M, pH 10) the hydrogen wave was shifted to more negative potentials and it was possible to detect nickel and cobalt.

4.1.1 Detection of nickel(II) in ammonia buffer and external standard calibration curves

The optimal voltammetric settings for the detection of nickel in ammonia buffer in the concentration range from 25 μg/L to 125 μg/L was determined as follows. Scan rate 15 mV/s, pulse amplitude 50 mV, voltage step 5 mV, pulse time 50 ms deposition potential - 1.2 V, deposition time 30 seconds, start potential -1.0 V, end potential 0.4 V.
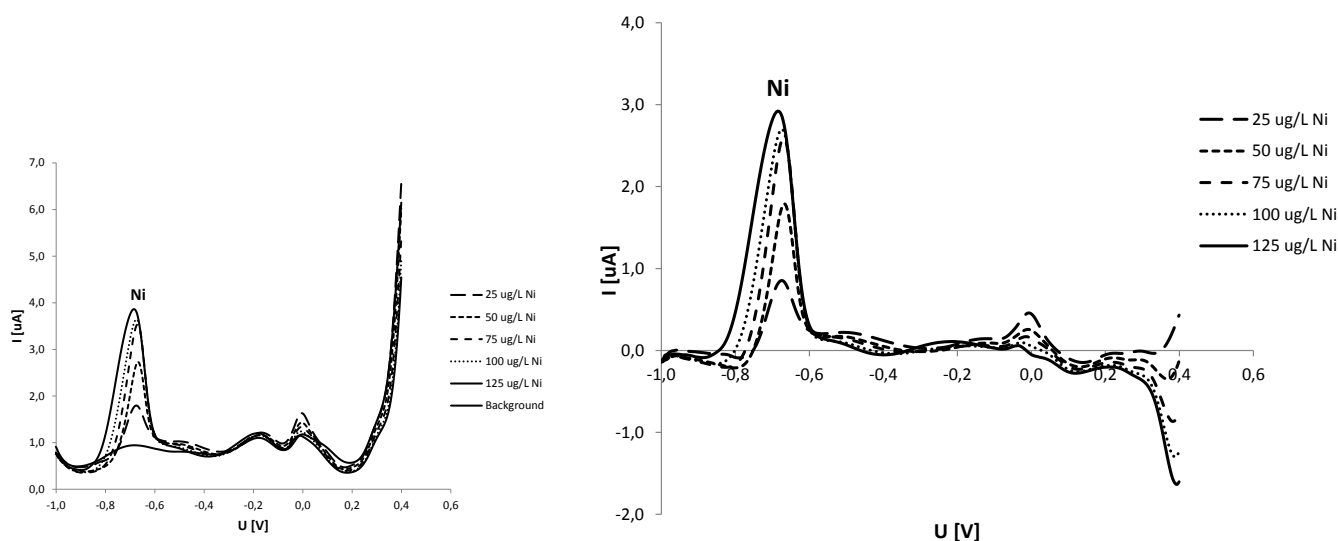
(a) Differnetial pulse anodic stripping voltamme-   (b) Subtractive differential pulse anodic stripping voltammetry
try

Figure 10: Detection of nickel(II) in ammonia buffer (0.01 M, pH 10) by differential pulse anodic stripping voltammetry, 10(a), and subtractive differential pulse anodic stripping voltammetry, 10(b). Scan rate 15 mV/s, pulse amplitude 50 mV, deposition potential - 1.2 V, deposition time 30 seconds, scan from -1.0 V to 0.4 V. Nickel standard solution (30 mg/L) has been successively added, 25 μ L at the time, to the ammonia buffer to create sample solutions of known nickel concentration. The nickel concentration ranges from 25 μg/L to 125 μg/L as indicated in the figure.

Figure 10, displays the voltammograms of the detection of nickel in ammonia buffer. Both the differential pulse anodic stripping voltammetry (DPASV) and subtractive differential pulse anodic stripping voltammetry (SDPASV) voltammograms are displayed. The voltammograms are the generated by successively adding 25 μL nickel standard solution (30 mg/L) to ammonia buffer to create calibration solutions of known nickel concentration that ranges from 25 μg/L to 125 μg/L. Figure 11 shows the external standard calibration curve for the detection of nickel in ammonia buffer for both DPASV and SDPASV, based on the analysis of the calibration solutions. The results were reproduced several times, as shown in Appendix C

As can be seen from Figure 11, the implementation of SDPASV did not improve the dynamic range of the calibration curve, nor the significance of the regression, compared to DPASV. The dynamic range ends at abut 75 $m u$g/L, and the coefficient of determination of the calibration curves is practically the same, for both methods. By visual inspection of the voltammograms in Figure 10 there is no apparent improvement in the symmetry
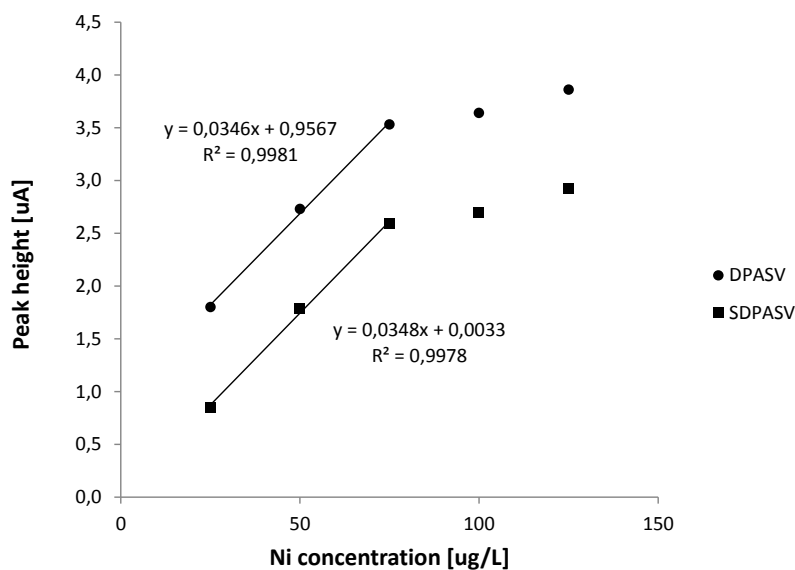
38

Figure 11: External standard calibration curve corresponding to the solutions analysed by differential pulse anodic stripping voltammetry and subtractive anodic stripping voltammetry as displayed in Figure 10. The linear dynamic range for detection of nickel in ammonia buffer ends at about 75 μg/L nickel, thus the correlation curve is conctructed using the three first calibration points (25 μg/L to 75 μg/L). The squared coefficient of determination (R^2) and the equation of the calibrations curves are given in the figure.

or the definition of the nickel peak by the SDPASV procedure. This is true for all the repetitions of the external calibration curve experiments, as shown in Appendix C. The SDPASV procedure requires that an additional scan of the background is recorded straight after the DPASV scan. The experimental conditions must be as equal as possible for the background scan and the DPASV scan for the SDPASV method to be most effective, which is not always easy to accomplish. Thus, it is considered unnecessary to employ the SDPASV method in this case because the DPASV scans alone yield good results.

Figure 12 displays a comparison of the three external calibration curves from the three repetitive DPASV external standard calibration experiments, as shown in Figure 10 and in Figures 53 and 55 in Appendix C. They all have the approximately the same slope, however, the intercepts differ. Two of the curves are quite similar in both slope and intercept, while the third has a substantially higher intercept. The calibration curve with the highest intercept was obtained with a slightly different procedure than the two other calibration curves. For the elevated calibration curve the DPASV scans were recorded immediately after polishing the electrode. While for the two other calibration curves the

electrode was scanned from -1.0 V to 0.4 V several times in pure ammonia buffer until a stable background was obtained, before the DPASV procedure began. This difference in experimental procedure can help to explain why the one calibration curve differs from the two other.

The deviation between the two most similar calibration curves is most likely caused by small difference in the concentration of the calibration solutions due to measurement uncertainties, and noise in the analytical signal.

All three calibration curves have a high coefficient of determination and are significant according to the F test. The residual plots are all homoscedastic. See Appendix A for calculations and residual plots. This indicates that there exists a linear relationship between the analyte response (peak height) and the concentration of nickel in the solution, and that it is appropriate to use a linear calibration curve to determine the nickel concentration of an unknown solution.
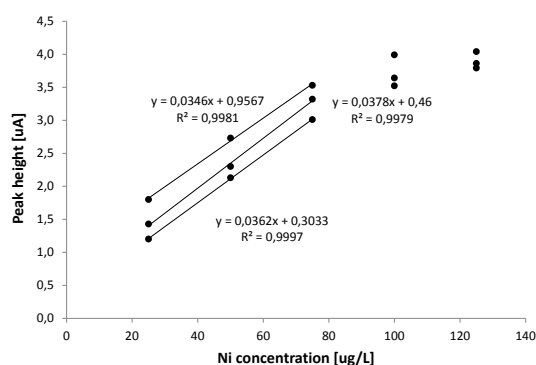

Figure 12: External standard calibration curves for the detection of nickel(II) in ammonia buffer (0.01 M, pH 10) by differential anodic stripping voltammetry. Nickel standard solution (30 mg/L) has been successively added, 25 μ L at the time, to the ammonia buffer to create sample solutions of known nickel concentration. The nickel concentration ranges from 25 μg/L to 125 μg/L as indicated in the figure. Scan rate 15 mV/s, pulse amplitude 50 mV, deposition potential - 1.2 V, deposition time 30 seconds, scan from -1.0 V to 0.4 V. The squared coefficient of determination (R^2) and the equation of each calibration curve is given in the figure. The linear dynamic range for detection of nickel in ammonia buffer by DPASV ends at about 75 μg/L nickel.

4.1.2 Detection of cobalt(II) in ammonia buffer and external standard calibration curves

The optimal voltammetric settings for the detection of nickel in ammonia buffer in the concentration range from 25 μg/L to 125 μg/L was determined as follows. Scan rate 15

(a) Differnetial pulse anodic stripping voltamme- (b) Subtractive differential pulse anodic strip-
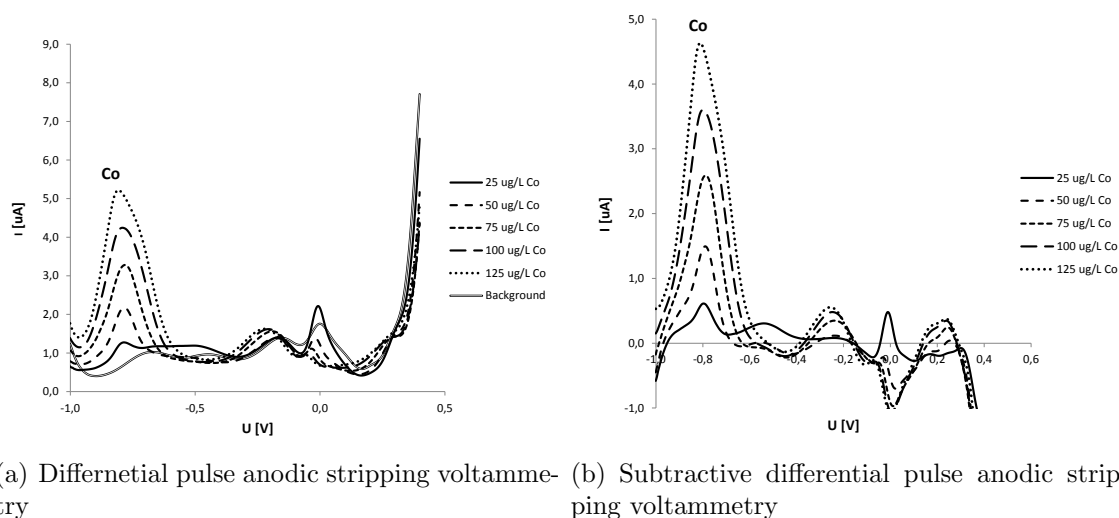try ping voltammetry

Figure 13: Detection of cobalt(II) in ammonia buffer (0.01 M, pH 10) by differential pulse anodic stripping voltammetry, 13(a), and subtractive differential pulse anodic stripping voltammetry, 13(b). Scan rate 15 mV/s, pulse amplitude 50 mV, deposition potential - 1.5 V, deposition time 100 seconds, scan from -1.0 V to 0.4 V. Cobalt standard solution (30 mg/L) has been successively added, 25 μ L at the time, to the ammonia buffer to create sample solutions of known nickel concentration. The nickel concentration ranges from 25 μg/L to 125 μg/L as indicated in the figure.

mV/s, pulse amplitude 50 mV, voltage step 5 mV, pulse time 50 ms deposition potential - 1.5 V, deposition time 100 seconds, start potential -1.0 V, end potential 0.4 V.

Figure 13, displays the detection of cobalt in ammonia buffer. Both the DPASV and SDPASV voltammograms are displayed. The voltammograms are the generated by successively adding 25 μL cobalt standard solution (30 mg/L) to ammonia buffer to create calibration solutions of known nickel concentration that ranges from 25 μg/L to 125 μg/L. Figure 14 shows the external standard calibration curve for the detection of cobalt in ammonia buffer for both DPASV and SDPASV, based on the analysis of the calibration solutions. The results were reproduced several times, as shown in Appendix C

As for the detection of nickel the detection of cobalt by the SDPASV method does not improve the external standard calibration curve, nor the symmetry and definition of the cobalt peak, compared to the simpler DPASV method. Thus, it is not necessary to use the SDPASV method to acquire good results.

Figure 15 displays three external calibration curves all constructed in the same way as the the DPASV external calibration curve in Figure 14. The calibration curves have similar
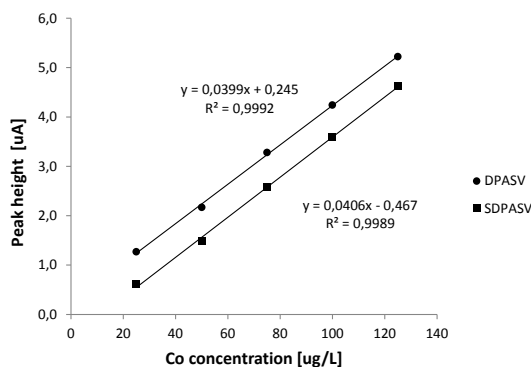
Figure 14: External standard calibration curve corresponding to the solutions analysed by DPASV and SDPASV as displayed in Figure 13. The squared coefficient of determination (R^2) and the equation of the calibration curves are given in the figure.

slopes and intercepts, but are not as parallel as the nickel calibration curves, see Figure 12. Care was taken to ensure that the experimental conditions were the same during all the calibration experiments. Thus, the experimental conditions should not have influenced the results significantly. However, it is very difficult to get the experimental conditions identical each time, so a small amount of the differences between the calibration equations may be caused by variations in the experimental conditions. The differences in the calibration curves may also be caused by inequalities in the concentration of the calibration solutions due to measurement uncertainties, and noise in the analytical signal.

The coefficient of determination of all three curves exceeds 0.98 and the calibration curves are all significant according to the F test. The residual plots are all homoscedastic, see Appendix A for calculations and residual plots. This indicates that there exists a linear relationship between the analyte response (peak height) and the concentration of cobalt in the solution, and that it is appropriate to use a linear calibration curve to determine the cobalt concentration of an unknown solution.

4.1.3 Separation of the joint nickel and cobalt peak by complexing agents

As can be seen from Figure 16, scan labeled *Without EDTA*, the simultaneous detection nickel and cobalt is impossible in ammonia buffer because the two peaks overlap. To try and separate the nickel and cobalt peaks five different complexing agents were tested. The selection of ligands was based on earlier studies of nickel and cobalt detection by voltammetric methods using complexing agents [34,35] and common complexing agents of nickel and cobalt [34,50]. EDTA, ammonia, potassium thiocyanate, citric acid, and glycine
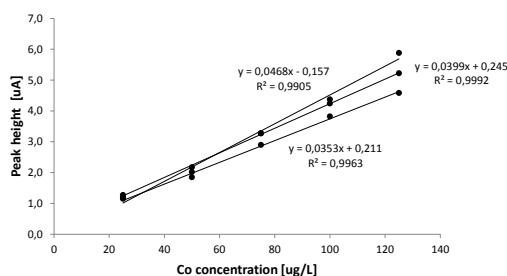
Figure 15: External standard calibration curves for the detection of nickel(II) in ammonia buffer (0.01 M, pH 10) by differential anodic stripping voltammetry. Cobalt standard solution (30 mg/L) has been successively added, 25 μ L at the time, to the ammonia buffer to create sample solutions of known nickel concentration. The cobalt concentration ranges from 25 μg/L to 125 μg/L as indicated in the figure. Scan rate 15 mV/s, pulse amplitude 50 mV, deposition potential - 1.5 V, deposition time 100 seconds, scan from -1.0 V to 0.4 V. The squared coefficient of determination (R^2) and the equation of each calibration curve is given in the figure.

are the five complexing agents that were tested. Each of the five figures below, display a comparison between DPASV scans in ammonia buffer added Ni(II) and Co(II) standard with and without a complexing agent. EDTA, ammonia, potassium thiocyanate, citric acid, and glycine are displayed in Figure 16, Figure 17, Figure 18, Figure 19 and Figure 20, respectively.

A compromise between the optimal voltammetric settings for detection of nickel in ammonia buffer and detection of cobalt in ammonia buffer was applied in all experiments utilizing complexing agents.The voltammetric settings were as follows. Scan rate 15 mV/s, pulse amplitude 50 mV, voltage step 5 mV, pulse time 50 ms deposition potential - 1.4 V, deposition time 65 seconds, start potential -1.0 V, end potential 0.4 V. The concentration of nickel and cobalt in all experiments were 50 μg/L

The addition of EDTA at a concentration of 4 μmol/L to the ammonia buffer makes the joint nickel and cobalt peak asymmetric and deformed. As the EDTA concentration increases the peak height decreases. However, the peak decreases faster on the right side, than on the left side. At an EDTA concentration of 5 μmol/L there is an indication of a very small elevation on the left side of the original peak compared to the right side of the peak. At an EDTA concentration of 6 μmol/L it seems like the starting peak at -0.7 V and peak height 2.5 μA has reduced to a small peak at about -0.8 V and peak height 1.5 μA. Compared to the cobalt peak from a DPASV scan in ammonia buffer containing the same amount of cobalt as in the solution added EDTA, the peaks appear at the same place in the voltammogram. Although the cobalt peak from the solution not containing EDTA is
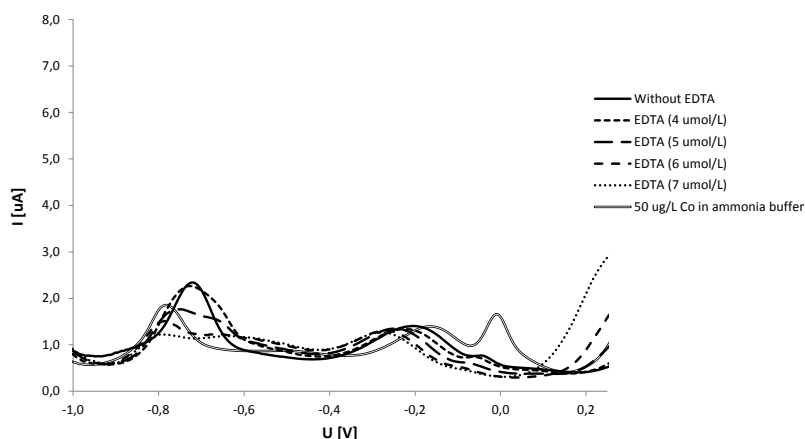
Figure 16: Differential pulse anodic stripping voltametry (DPASV) scans carried out in ammonia buffer solution (0.01 M, pH 10) containing nickel(II) and cobalt(II) (0.85 $\mu mol/L$), and EDTA. The EDTA concentration ranges from $4\mu mol/L$ to $7\mu mol/L$. Scan rate 15 mV/s, pulse amplitude 50 mV, deposition potential - 1.2 V, deposition time 100 seconds, scan from -1.0 V to 0.4 V. For comparison a DPASV scan in ammonia buffer (0.01 M, pH 10) containing nickel(II) and cobalt(II) (0.85 $\mu mol/L$) without EDTA is shown, scan rate 15 mV/s, pulse amplitude 50 mV, deposition potential - 1.4 V, deposition time 65 seconds, scan from -1.0 V to 0.4 V.

higher, the two peaks have approximately the same peak potential, -0.8 V. Thus,it seems like the addition of EDTA, at the right concentration, could be used to completely remove the nickel signal and detect cobalt alone. Here, the concentration ratio between EDTA and cobalt is six to one, when the peak assumed to be solely due to the cobalt in solution, is most pronounced. However, the peak is removed completely when the EDTA concentration reaches 7 μmol/L, such that the EDTA concentration must be carefully adapted to the cobalt and nickel concentration in the sample. This would be very difficult in an on-line analysis of nickel and cobalt in waste water, where the metal concentrations will fluctuate.

Addition of ammonium hydroxide to the ammonia buffer solution increases the peak height and shifts the peak to a more negative potential. However, there is no indication of separation of the peak into two separate cobalt and nickel peaks.

A KSCN concentration of 1.7 μmol/L in the synthetic cobalt and nickel solutions only flattens the combined cobalt and nickel peak. At a concentration of 20 μmol/L there is a small shoulder at the left side of the peak, indicating a better separation of the two metals when KSCN is added than in ammonia buffer alone. However, the shoulder is to small to be used for quantitative purposes.

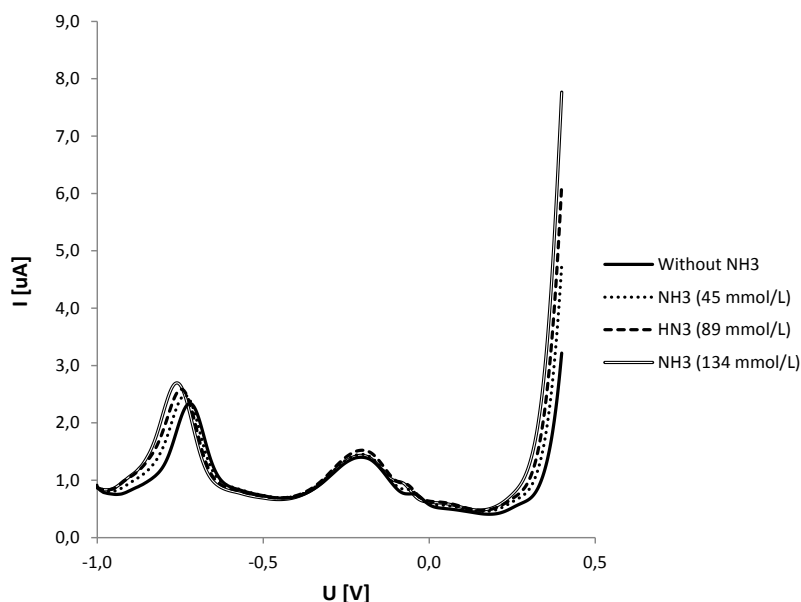Citric acid in ammonia buffer containing nickel and cobalt only broadens the peak.

Figure 17: Differential pulse anodic stripping voltametry (DPASV) scans carried out in ammonia buffer solution (0.01 M, pH 10) containing nickel(II) and cobalt(II) (0.85 $\mu mol/L$), and ammonia. The ammonia concentration ranges from 45 mmol/L to 134 mmol/L. Scan rate 15 mV/s, pulse amplitude 50 mV, deposition potential - 1.4 V, deposition time 65 seconds, scan from -1.0 V to 0.4 V. For comparison a DPASV scan in ammonia buffer (0.01 M, pH 10) containing nickel(II) and cobalt(II) (0.85 $\mu mol/L$) without added ammonia is shown, scan rate 15 mV/s, pulse amplitude 50 mV, deposition potential - 1.4 V, deposition time 65 seconds, scan from -1.0 V to 0.4 V.

Glycine is the complexing agent that gives the best separation between cobalt and nickel in ammonia buffer of all the complexing agent used in this study. A concentration below 30 μmol, when the cobalt and nickel concentration is 0.85 μmol/L, seems to be preferable. At a glycine concentration of 30 μmol/L the shoulder on the left side of the peak diminishes considerably compared to the shoulder on the peak in the voltamograms at lower glycine concentration.

Figure 20 displays two scans in solutions with a 10 μmol/L glycine concentration that differ substantially. The only difference between these two scans is the amount of scans that have been performed between polishing of the electrode and the scan of interest. Before the scan that has the most pronounced shoulder was recorded, six scans in ammonia buffer with a cobalt concentration 50 μmol/L and varying glycine concentration had been performed. The deposition potential in these scans were -1.4 V and the deposition time was 65 seconds. Before the second scan that has a less pronounced shoulder was recoded two scans in ammonia buffer at a cobalt and nickel concentration of 50 μmol/L and a glycine
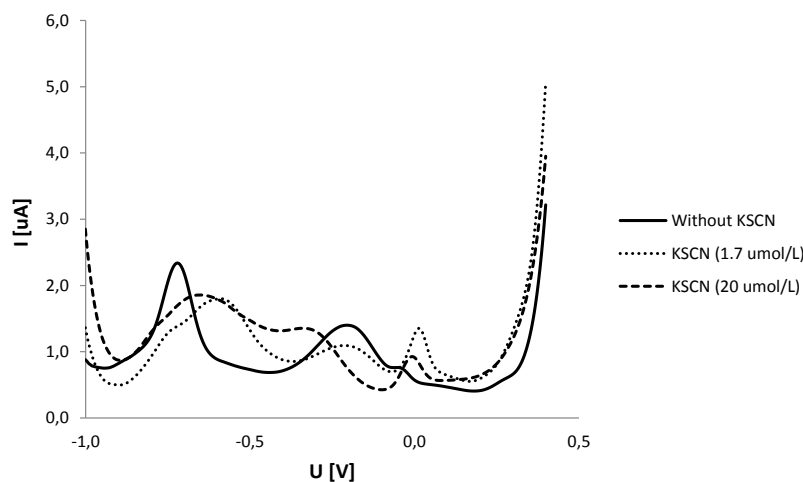
45

Figure 18: Differential pulse anodic stripping voltametry (DPASV) scans carried out in ammonia buffer solution (0.01 M, pH 10) containing nickel(II) and cobalt(II) (0.85 $\mu mol/L$), and KSCN. The KSCN concentration ranges from 1.7$\mu mol/L$ to 20$\mu mol/L$. Scan rate 15 mV/s, pulse amplitude 50 mV, deposition potential - 1.4 V, deposition time 65 seconds, scan from -1.0 V to 0.4 V. For comparison a DPASV scan in ammonia buffer (0.01 M, pH 10) containing nickel(II) and cobalt(II) (0.85 $\mu mol/L$) without added KSCN is shown, scan rate 15 mV/s, pulse amplitude 50 mV, deposition potential - 1.4 V, deposition time 65 seconds, scan from -1.0 V to 0.4 V.

concentration of 10 μmol/L had been performed. The deposition potential in these scans were -1.4 V and the deposition time was 30 seconds. Thus, is seems like the analytical signal of cobalt increases as the number of prior scans in solution containing cobalt increases. This can be caused by incomplete removal of deposited cobalt from the previous scans, which may be counteracted by implementing a electrochemical or mechanical cleaning procedure between each scan.

The deposition potential in these scans were -1.4 V and the deposition time was 65 seconds. Before the scan in ammonia buffer with a glycine concentration of 30 μmol/L was recorded the exact same scans as before the scan at glycine concentration of 10 μmol/L with the most pronounced shoulder scan was performed. Thus, these two scans can be compared. Which makes it possible to decide that a glycine concentration of 10 μmol/L is more favourable than a glycine concentration of 30 μmol/L.

After polishing and before the scan with glycine concentration 2 μmol/L was recorded three scans in ammonia buffer with nickel concentration of 50 μmol/L and varying glycine concentration had been performed. These differ from the scans that had been performed
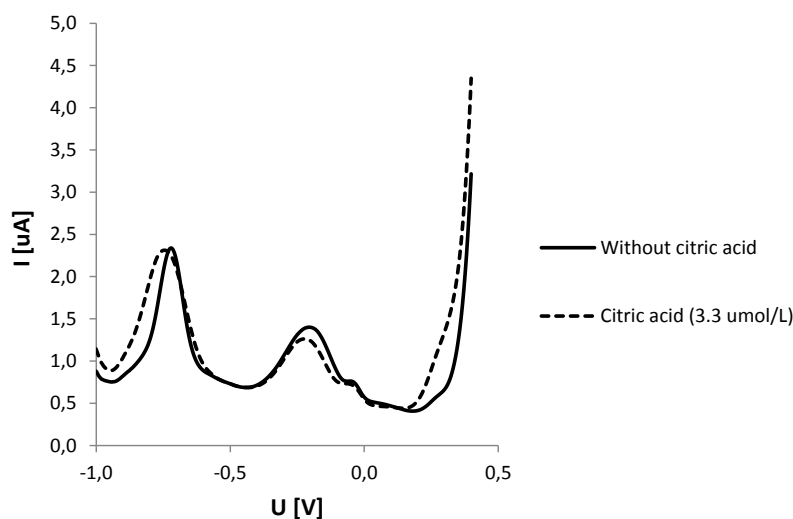
Figure 19: Differential pulse anodic stripping voltametry (DPASV) scans carried out in ammonia buffer solution (0.01 M, pH 10) containing nickel(II) and cobalt(II) (0.85 $\mu mol/L$), and citric acid (3.3$\mu mol/L$). Scan rate 15 mV/s, pulse amplitude 50 mV, deposition potential - 1.4 V, deposition time 65 seconds, scan from -1.0 V to 0.4 V. For comparison a DPASV scan in ammonia buffer (0.01 M, pH 10) containing nickel(II) and cobalt(II) (0.85 $\mu mol/L$) without added KSCN is shown, scan rate 15 mV/s, pulse amplitude 50 mV, deposition potential - 1.4 V, deposition time 65 seconds, scan from -1.0 V to 0.4 V..

prior to two scans at glycine concentration 10 μmol/L in that there is no cobalt in the solution that were used. Therefore, it is not appropriate to determine if 2 μmol/L or 10 μmol/L glycine concentration is more favourable.

Figure 21(a) displays detection of cobalt and nickel by differential pulse anodic stripping voltammetry in ammonia buffer (0.01 M, pH 10) added glycine. The scan was recorded right after mechanical polishing of the electrode followed by several scans in pure ammonia buffer (0.01 M, pH 10) to obtain a stable background. This was done to see if the cobalt shoulder on the joint nickel and cobalt peak could be detected if a mechanical cleaning step is performed between each scan. The cobalt and nickel concentration were both 50 μg/L and the glycine concentration was 10 μmol/L. The deposition potential was -1.45 V and the deposition time 30 seconds. The cobalt shoulder on the peak is small. However, the cobalt shoulder is enhanced when subtractive differential pulse anodic stripping voltammetry is applied, as can be seen in Figure 21(b).

Thus, a combination of mechanical cleaning between each scan and SDPASV could be used to simultaneously detect nickel and cobalt in ammonia buffer added glycine. Alternatively,
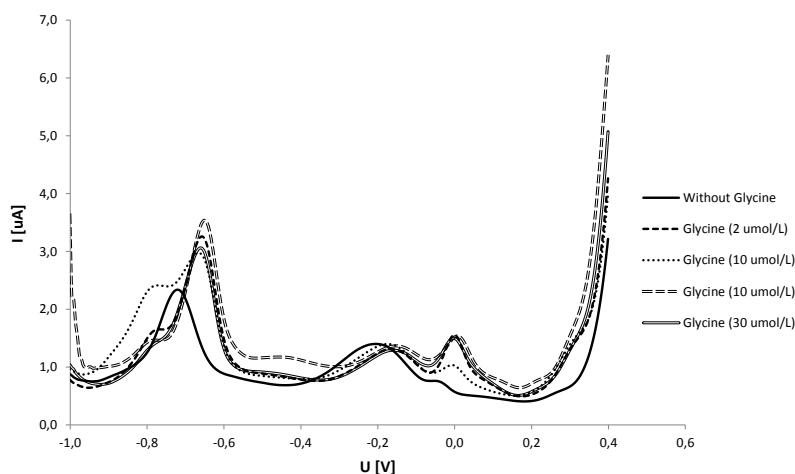
Figure 20: Differential pulse anodic stripping voltametry (DPASV) scans carried out in ammonia buffer solution (0.01 M, pH 10) containing nickel(II) and cobalt(II) (0.85 $\mu mol/L$), and glycine. The glycine concentration ranges from $2\mu mol/L$ to $30\mu mol/L$. Scan rate 15 mV/s, pulse amplitude 50 mV, deposition potential - 1.4 V, deposition time 65 seconds, scan from -1.0 V to 0.4 V. For comparison a DPASV scan in ammonia buffer (0.01 M, pH 10) containing nickel(II) and cobalt(II) (0.85 $\mu mol/L$) without added glycine is shown, scan rate 15 mV/s, pulse amplitude 50 mV, deposition potential - 1.4 V, deposition time 65 seconds, scan from -1.0 V to 0.4 V.

a SDPASV procedure utilizing a given number of consecutive scans to "grow" the cobalt shoulder could be applied. This procedure would most likely enhance the sensitivity of the method and the separation of the two peaks. The electrode must be cleaned between analyses in this procedure too.

4.2 Nickel and cobalt detection in waste water from the nickel refinery

As explained earlier it was decided to detect nickel and cobalt as one peak in the waste water from the nickel refinery. The optimal voltammetric settings for the detection of nickel and cobalt in waste water was determined as follows. Scan rate 15 mV/s, pulse amplitude 50 mV, voltage step 5 mV, pulse time 50 ms deposition potential - 1.0 V, deposition time 350 seconds - 600 seconds depending on the concentration of nickel and cobalt in the waste water sample, start potential -1.0 V, end potential 0.4 V, dilution ratio one part waste water to five parts ammonia buffer.

To activate and stabilize the gold electrode, the electrode was held at at potential of 0.9 V
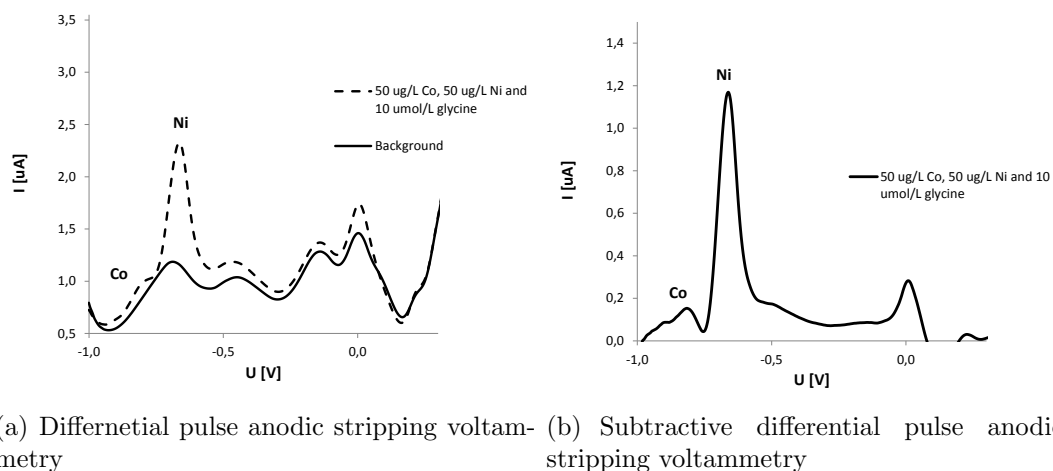
(a) Differnetial pulse anodic stripping voltammetry

(b) Subtractive differential pulse anodic stripping voltammetry

Figure 21: Detection of cobalt(II) and nickel(II) in ammonia buffer (0.01 M, pH 10) containing glycine (10 μmol/L) by differential pulse anodic stripping voltammetry, 21(a), and subtractive differential pulse anodic stripping voltammetry, 21(b). Scan rate 15 mV/s, pulse amplitude 50 mV, deposition potential - 1.45 V, deposition time 100 seconds, scan from -1.0 V to 0.4 V.

for 30 seconds before a couple of scans from -0.9 V to 0.4 was performed. Both steps of the pretreatment procedure were carried out in a solution of waste water and ammonia buffer. Then the solution was changed to a new solution of ammonia buffer and waste water, and a differential pulse anodic stripping voltammetry scan was recorded. This procedure was repeated until the the electrode response was stable, about five to six times.

It was also found important to change the sample solution between each analysis to ensure reproducibility of the results. Figure 22 shows the voltammograms from four analyses carried out in the same solution. The nickel and cobalt peak is not reproducible and the baseline increases in the anodic part of the voltammograms. In addition the peak at 0 V increases. The fifth voltammogram in the figure displays a scan carried out after the sample solution has been changes. The baseline is still not back to normal. Thus, cleaning or reactivation of the electrode is necessary after several scans in the same solution. The observed, effect could be caused by changes in the pH of the solution due to hydrogen evolution during the deposition step. Or other changes in the solution matrix as a result of the consecutive DPASV scans

4.2.1 Reproducibility of the results

Figure 23 shows voltammograms for the analysis of the first supply of waste water from the nickel refinery by differential pulse anodic stripping voltammetry.
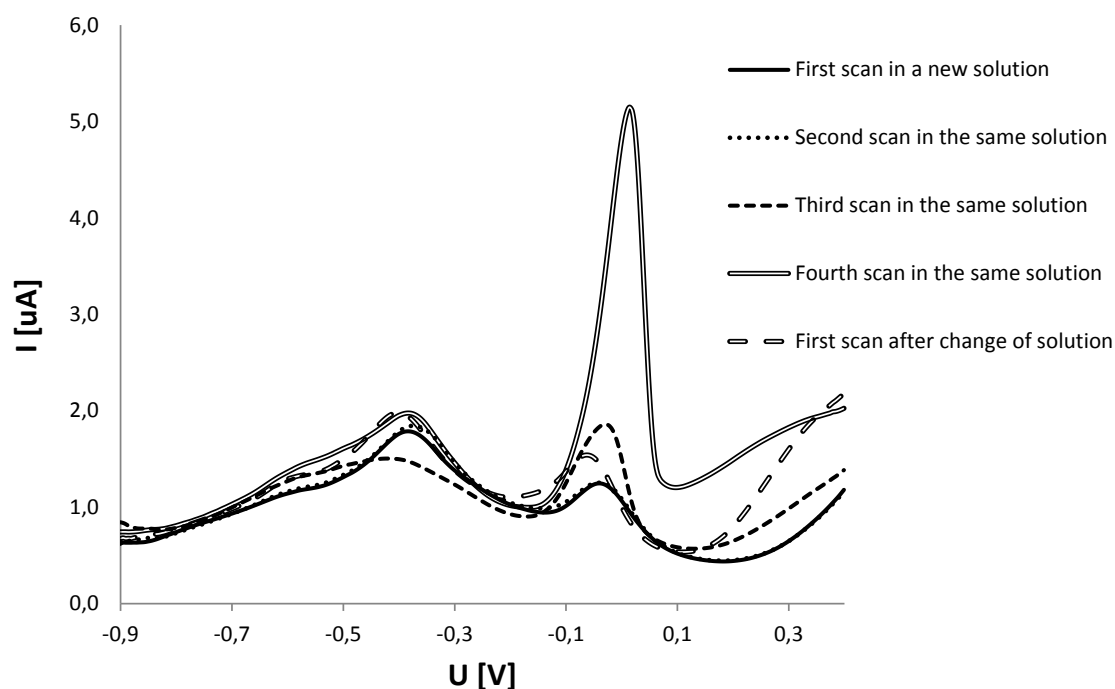
Figure 22: Voltammograms from four DPASV analyses of waste water carried out without changing the sample soltution betwen each scan, and one scan carried out after the solution has been changed. The sample has been diluted with ammonia buffer (0.01 M, pH 10), one part sample to five parts ammonium buffer. Scan rate 15 mV/s, pulse amplitude 50 mV, deposition potential - 1.0 V, deposition time 500 seconds, scan from -0.9 V to 0.4 V.

In Figure 23 it can bee seen that the joint nickel and cobalt peak in three first scans have almost identical peak heights and that the three voltammograms all lie on top of each other. The peak height in the fourth scan however, is higher. The peak height of the joint nickel and cobalt peak continues to increase in scan five, before it decreases slightly in the three last scans. In the three last scans the peak height is very similar. At first it seems like there is a trend of increasing peak height during the analysis. However, from the fifth scan to the three last scans the peak height decreases. Thus, the differences could be due to random error such as uncertainties of the dilution of the samples, or inaccuracy in the measurement caused by the equipment and wires.

To examine the observed differences in peak height more thoroughly the eight scans were divided into two sets, the four fist scans in one set and the four last scans in a second set, before a two tailed hypothesis test on the two experimental means of the sets was carried
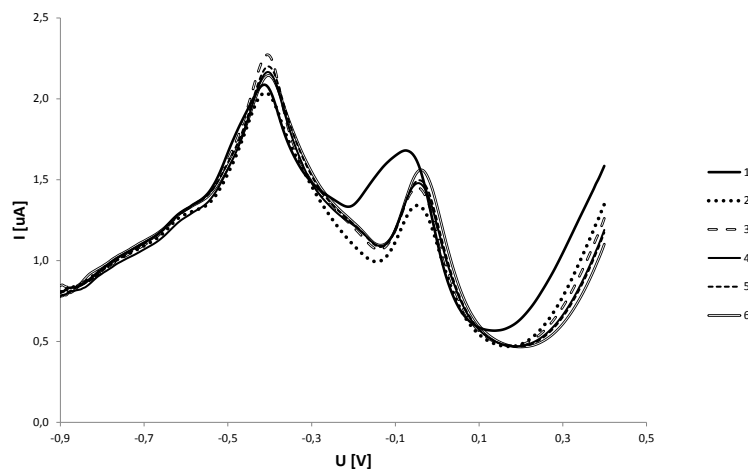
Figure 23: Nine repetitions of the detetction of nickel(II) and cobalt(II) in nickel plant waste water sample by differential pulse anodic stripping voltammetry. The sample has been diluted with ammonia buffer (0.01 M, pH 10), one part sample to five parts ammonium buffer. Scan rate 15 mV/s, pulse amplitude 50 mV, deposition potential - 1.0 V, deposition time 500 seconds, scan from -0.9 V to 0.4 V. The scan order is given in the legend to the right of the voltammograms.

out. At a significance level of 0.100 the the null hypothesis is accepted. The P-value is 0.32. See Appendix B for details on the calculations. Thus, the hypothesis test concludes, down to a significance level of 0.32, that the two sets of data come from the same population. In other words, it is possible to observe the amount of variation in peak height, that has been observed here in the analysis of the waste water sample by DPASV, although it is the same sample that is analysed continuously. The result of the hypothesis test and the fact that the peak height does not increase constantly, supports the notion that the variation in peak height is due to random error.

Effect of storage of the gold electrode in rinsed water Figure 24 displays the voltammograms from analysis of another waste water sample from the nickel refinery by DPASV. This sample was analysed immediately after the analysis of the waste water sample, whose voltammograms are shown in Figure 23, without any pretreatment or mechanically cleaning of the electrode, and at the same experimental conditions.

Unlike the voltammograms in Figure 23, the peak height of the joint nickel and cobalt peak in voltammograms in this Figure 24 show no apparent trend of increasing or decreasing peak height. There is a small difference in peak height between each peak, however the peak heights increase or decrease from one scan to another randomly. By visual inspection
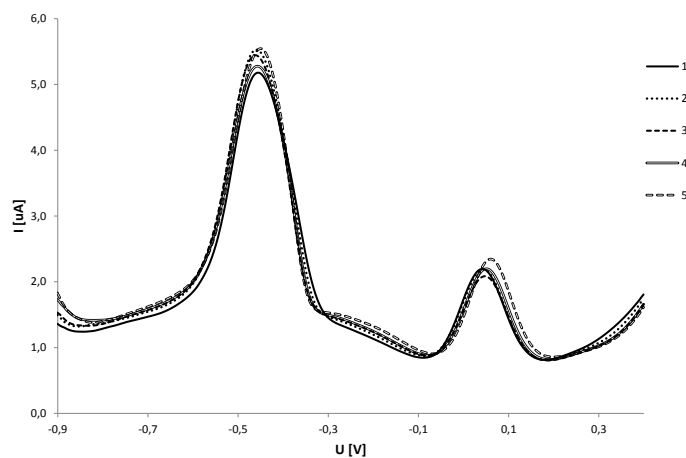
Figure 24: Nine repetitions of the detetction of nickel(II) and cobalt(II) in nickel plant waste water sample by differential pulse anodic stripping voltammetry. The sample has been diluted with ammonia buffer (0.01 M, pH 10), one part sample to five parts ammonium buffer. Scan rate 15 mV/s, pulse amplitude 50 mV, deposition potential - 1.0 V, deposition time 500 seconds, scan from -0.9 V to 0.4 V. The scan order is given in the legend to the right of the voltammograms.

it can be seen that the average peak height in Figure 24 is more than twice the average peak height in Figure 23. Thus, it is likely that the peak height in Figure 23 is more affected by noise in the analytical signal, because the ratio between analytical signal and noise decreases. This would also help explain the larger variation in peak height when the measured signal is lower, as observed in Figures 23 and 24.

After storing the gold electrode in rinsed water over night, the nickel and cobalt measurements in waste water were repeated. The fist differential pulse anodic stripping voltammetry scan carried out under the exact same conditions as the scans that were carried out the previous day. The voltammogram from the first scan was very similar to the voltammograms in Figure 24. The joint nickel and cobalt peak is only slightly narrower than in the voltammograms obtained the previous day, but the peak height is the same. However, during the next repetitions of the experiment the peak height increases every time. Figure 25 compares the two sets of measurements.

The deposition time was reduced from 500 seconds to 350 seconds, which reduced the peak height of the joint nickel and cobalt peak down to the same peak height as in voltammograms from the previous day, as shown in Figure 26. The nickel-cobalt peak is narrower and the peak appearing at about 0.1 V is reduced considerably in the second set of measurements. As can be seen from Figure 27 the peak at 0.1 V is diminished when the
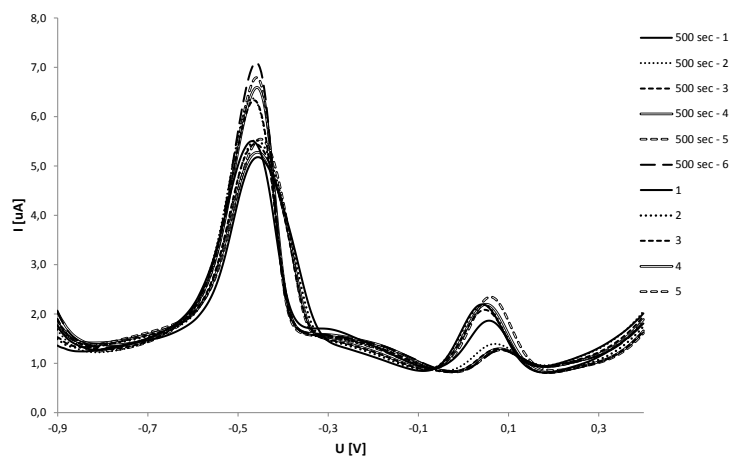
Figure 25: Comparisons of the voltammograms from the two analyses of nickel refinery waste water carried out before and after storage of the gold electrode in rinsed water over night. The scans labeled 1 5 refer to the scans performed the previous day, they are the same as the scans displayed in Figure 24. The scans labeled 500 sec - 1 to 500 sec - 6 refer to the second set of measurements that were performed after overnight storage of the gold electrode in rinsed water. The experimental conditions were the same for both sets. The samples were diluted with ammonia buffer (0.01 M, pH 10), one part sample to five parts ammonium buffer. Scan rate 15 mV/s, pulse amplitude 50 mV, deposition potential - 1.0 V, deposition time 500 seconds, scan from -0.9 V to 0.4 V. The scan order is given in the legend to the right of the voltammograms.

electrode is kept at 0.9 V for 10 seconds. This seems similar to what has happened when the electrode was stored in rinsed water over night.

After storage in rinsed water the electrode was transferred directly into a solution of one part waste water and five parts ammonia buffer, and scanned from -0.9 V to 0.4 V several times. It seems like this treatment of the electrode leads to an activation of the electrode in the same manner as applying an anodic potential to the electrode for a short amount of time does.

Figures 28 and 29 show the voltammograms for the two repetitive analysis of four different waste water samples from the nickel refinery by DPASV. The analyses was performed after activation of the electrode as described in section above.

To check if the results of the two repetitive analyses of each of the four waste water samples could be regarded as members of the same population, a two tailed hypothesis test on the two experimental means of the two sets of data for each waste water solution was carried out. See Appendix B for calculations.
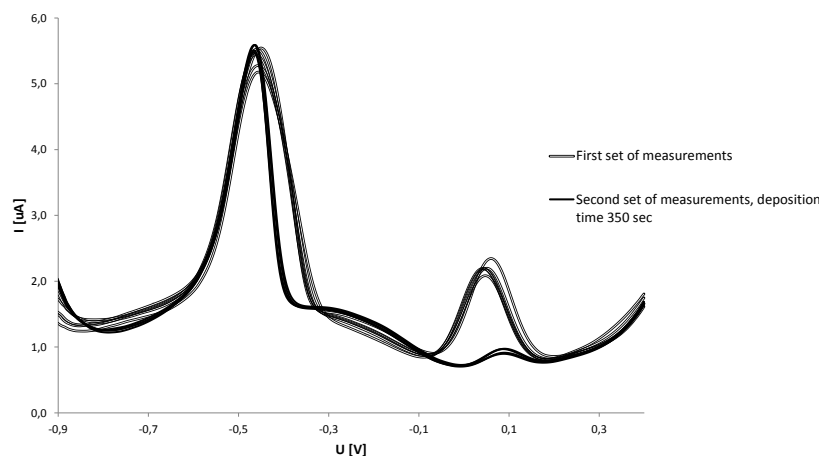
Figure 26: Comparisons of the voltammograms from the two analyses of nickel refinery waste water carried out before and after storage of the gold electrode in rinsed water over night. The scans labeled *First set of measurements* refer to the scans performed the previous day, they are the same as the scans displayed in Figure 24. The scans labeled *Second set of measuremnts, deposition time 350 sec* refer to the second set of measurements that were performed after overnight storage of the gold electrode in rinsed water, and after the deposition time had been reduced to 350 seconds. The experimental conditions were the same for both sets, except for the deposition time. The samples were diluted with ammonia buffer (0.01 M, pH 10), one part sample to five parts ammonium buffer. Scan rate 15 mV/s, pulse amplitude 50 mV, deposition potential - 1.0 V, deposition time 500 seconds, or 350 seconds (see legend), scan from -0.9 V to 0.4 V.

The null hypothesis is accepted at a significance level of 0.05 for the waste water solution of concentration 0.20 mg/L Ni and 0.36 mg/L Ni. Supplied by P values of 0.48 and 0.30, respectively there is fairly strong statistical evidence to support that it is possible to observe the amount of variation in peak height, that has been observed here in the analysis of the waste water sample by DPASV, although it is the same sample that is analysed repetitively. For these two solutions there is a 30 % chance or more that the test statistic will take on a value at least as extreme as the ones observed here when the null hypothesis is true.

However, for the solutions of nickel concentration 0.047 mg/L and 0.25 the null hypothesis is rejected at a significance level of 0.05. There is only a 6.5 % and 2.5 % chance, respectively, that the test statistic will take on a value at least as extreme as the ones observed here when the null hypothesis is true. Thus, the statistical evidence supporting the null hypothesis are not very strong for these solution.

To investigate the presence of any trends of increasing or decreasing peak height during
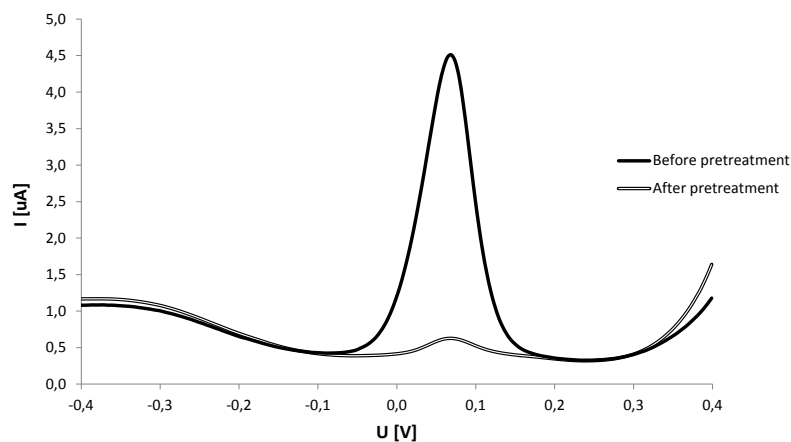
Figure 27: Comparisons of the voltammograms of two background scans from -0.9 V to 0.4 V in waste water diluted with ammonia buffer, dilution ratio one to five, before and after activation. The activation procedure consisted of keeping the electrode at 0.9 V for 10 seconds.

each of the two repetitive analyses of the four waste water solutions the scan order for each solution for each analysis was plotted. The scan orders for each waste water solution for the first and second analysis are shown in Figures 30 and 31, respectively.

In the first parallel of nickel and cobalt detection in waste water from the nickel refinery, Figure 30, the voltammograms from the analysis of the 0.47 mg/L nickel solution are practically identical. The analyses of the 0.36 mg/L nickel and the 0.25 mg/L nickel solutions both produced one voltammogram with a higher peak than the others, and three virtually identical voltammograms. It was the first scan that yielded the highest peak in both cases. The voltammograms from the analysis of the 0.20 mg/L nickel solution showed increasing peak height for each scan.

In the second parallel of nickel and cobalt detection in waste water from the nickel refinery, Figure 31, the peak height in the voltammograms from the analysis of the 0.47 mg/L nickel solution increase for the three first scans. However, the third and the fourth scan are identical. The analyses of the three remaining solutions all produced voltammograms with decreasing peak height for each scan.

Because of the large variation in peak height in the analysis of the 0.47 mg/L nickel solution and the trend of decreasing peak height during the analyses of the rest of the solutions it is could be helpful to implement a cleaning and stabilisation procedure between the two parallels waste water of analyses.
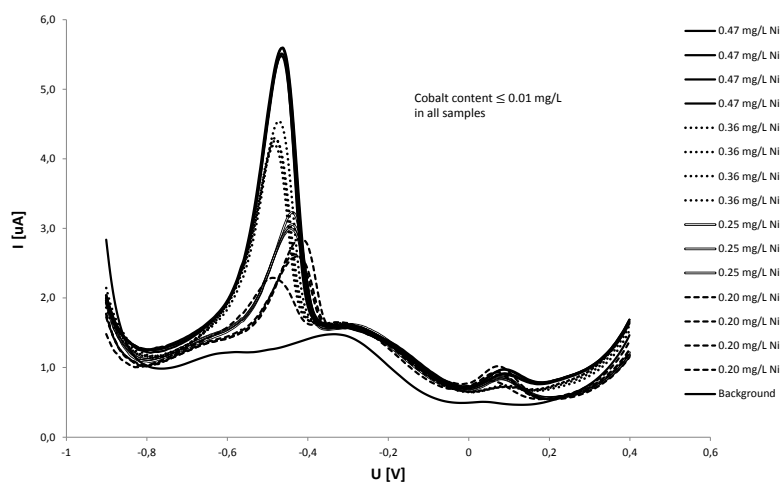
Figure 28: Detetction of nickel(II) and cobalt(II) in nickel plant waste water sample by differential pulse anodic stripping voltammetry. The samples have been diluted with ammonia buffer (0.01 M, pH 10), one part sample to five parts ammonium buffer. Scan rate 15 mV/s, pulse amplitude 50 mV, deposition potential - 1.0 V, deposition time 350 seconds, scan from -0.9 V to 0.4 V. Four different samples have been analysed, four times each in random order. The concentration of each sample, provided by the laboratory department at the nickel plant, is stated in the figure.

4.2.2 Standard addition calibration curve

Figure 32 shows the standard addition calibration curve for the detection of nickel and cobalt by differential pulse anodic stripping voltammetry in a waste water sample from the nickel refinery. The statistical calculations applicable to the generation and validation of the calibration curve are shown in Appendix A.

The concentration of nickel in the waste water sample used to generate the calibration curve is more than eighteen times higher than the cobalt concentration in the sample (values provided from the analysis department at the nickel refinery). Thus, the standard addition curve is generated by addition of nickel standard solution only. The contribution to the analytical signal from cobalt in solution is considered negligible.

The coefficient of determination of the standard addition calibration curve is close to one, which means that the linear calibration curve fits the data well. The residual plot is homoscedastic, which also help support the assumption that it is appropriate to fit a linear calibration curve to the data. The F value, 8517, is very large compared to the critical F value, 18.51, at a significance level of 0.05. Thus, according to the F test the regression is significant. It therefore seems to be appropriate to assume that there is a linear relationship
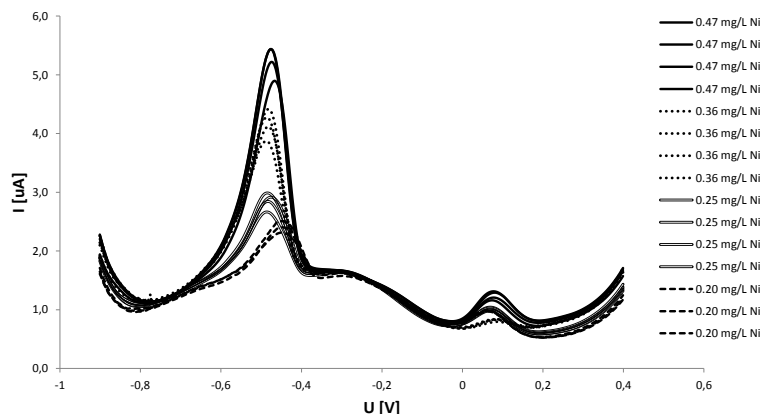
Figure 29: Detetction of nickel(II) and cobalt(II) in nickel plant waste water sample by differential pulse anodic stripping voltammetry. The samples have been diluted with ammonia buffer (0.01 M, pH 10), one part sample to five parts ammonium buffer. Scan rate 15 mV/s, pulse amplitude 50 mV, deposition potential - 1.0 V, deposition time 350 seconds, scan from -0.9 V to 0.4 V. Four different samples have been analysed, four times each in random order. The concentration of each sample, provided by the laboratory department at the nickel plant, is stated in the figure.

between the measured response and the concentration of nickel in the sample.

From the standard addition curve the concentration of the undiluted waste water sample is determined to be 0.21 mg/L $\pm$ 0.012 mg/L. The concentration of the sample as provided from the analysis department at the nickel refinery is 0.18 mg/L nickel, a difference of 0,03 mg/L or approximately 15 %.

When the DPASV method used to analyse the waste water, the joint nickel and cobalt concentration is measured. The laboratory department at Glencore Nikkelverk measures the two metals separately. Thus, small contributions to the analytical signal from cobalt in the waste water solution may help explain why the nickel concentration meaured by DPASV is higher. However, since nothing is known about the uncertainty associated with the result provided by Glencore Nikkelverk it is hard compare the two results further.
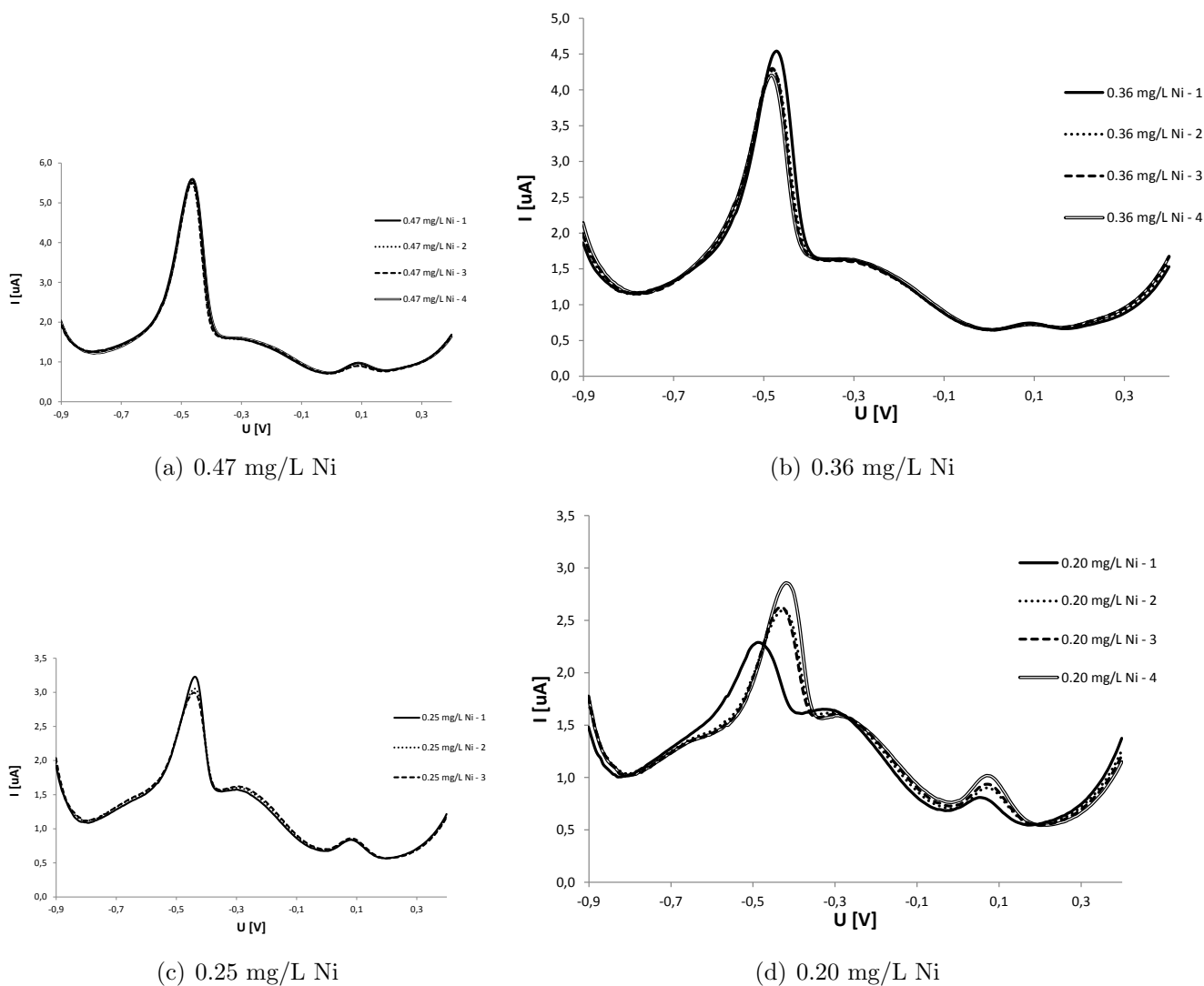
(a) 0.47 mg/L Ni

(b) 0.36 mg/L Ni

(c) 0.25 mg/L Ni

(d) 0.20 mg/L Ni

Figure 30: Voltammograms from the first analyses of four waste water samples from the nickel refiner by DPASV. The scan order for each solution is given in the legend. Scan rate 15 mV/s, pulse amplitude 50 mV, deposition Deposition potential - 1.0 V, deposition time 350 seconds, scan from -0.9 V to 0.4 V. The samples were diluted with ammonia buffer (0.01 M, pH 10), one part sample to five parts ammonium buffer

(a) 0.47 mg/L Ni

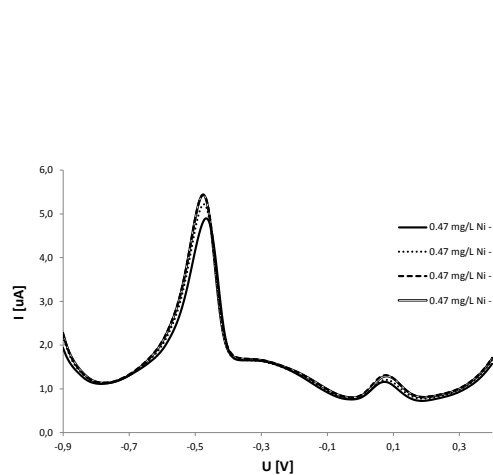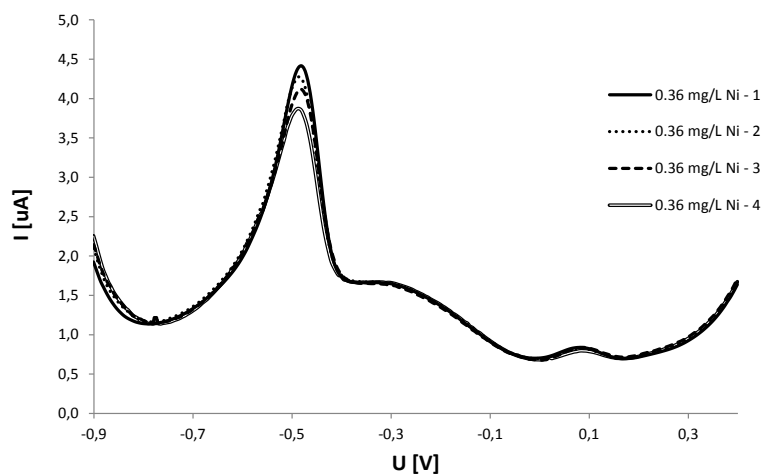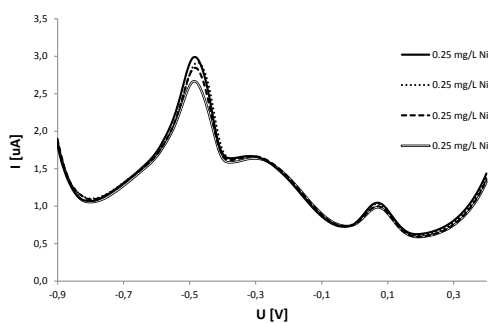(b) 0.36 mg/L Ni

(c) 0.25 mg/L Ni

(d) 0.20 mg/L Ni

Figure 31: Voltammograms from the second analyses of four waste water samples from the nickel refiner by DPASV. The scan order for each solution is given in the legend. Scan rate 15 mV/s, pulse amplitude 50 mV, deposition Deposition potential - 1.0 V, deposition time 350 seconds, scan from -0.9 V to 0.4 V. The samples were diluted with ammonia buffer (0.01 M, pH 10), one part sample to five parts ammonium buffer
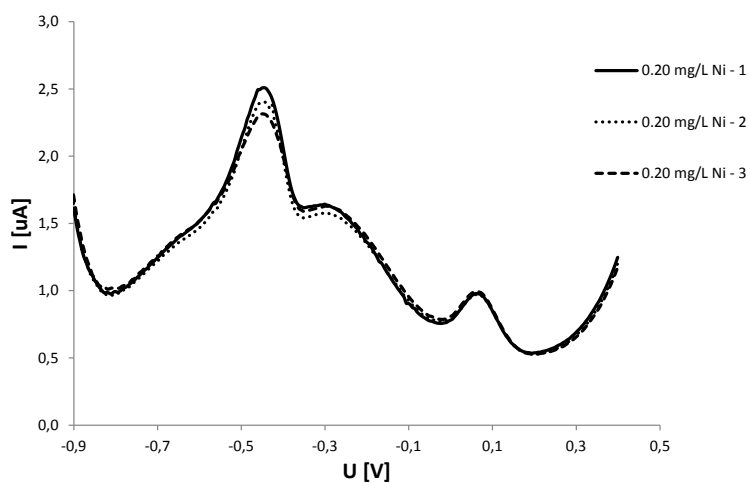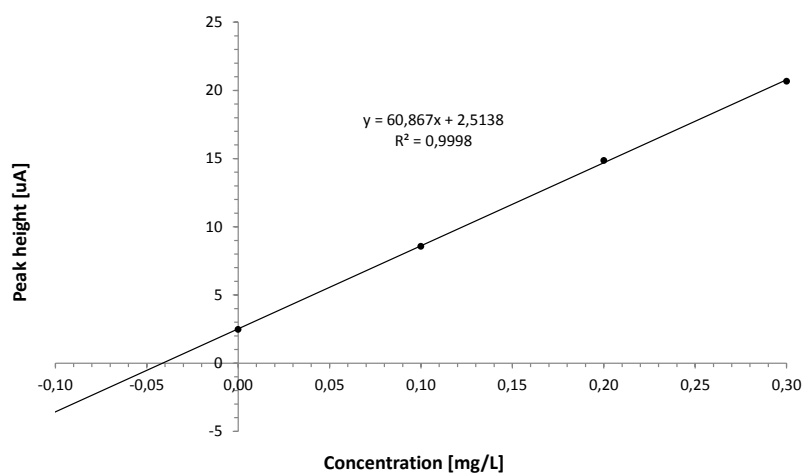
Figure 32: Standard addition calibration curve for the detection of nicke by differential pulse anodic stripping voltammetry in a waste water sample from the nickel refinery. 100 μL nickel standard (30 $\mu L/g$) was added to the waste water sample and analysed by differential pulse anodic stripping voltammetry. This procedure was repeated three times. The squared coefficient of determination (R^2) and the equation of the calibration curve is given in the figure. Extrapolation of the calibration curve to zero added nickel-standard is used to find the concentration of the waste water sample. The sample has been diluted with ammonia buffer (0.01 M, pH 10), one part sample to five parts ammonium buffer. Scan rate 15 mV/s, pulse amplitude 50 mV, deposition potential - 1.0 V, deposition time 350 seconds, scan from -0.9 V to 0.4 V. Analysis of the waste water sample at the laboratory at Glencore Nikkelverk determined the nickel concentration in the waste water to be 0.18 mg/L

5   Conclusion and Further Work

Control of the pH of the solution in which nickel(II) and cobalt(II) is to be detected is very important, otherwise the hydrogen wave will hide the peak of cobalt and nickel. The working window of the gold electrode in neutral or acidic solution was found to be too restricted in the cathodic direction for detection of the two metals by differential pulse anodic stripping voltammetry (DPASV). In solutions of pH ten and above the hydrogen wave is shifted far enough down in to the cathodic potential area for nickel and cobalt detection to be possible. However, this does not mean that nickel and cobalt can be measured by DPASV in any type of electrolyte solution of pH ten and above because the kinetics of the deposition of metals on the electrode is highly dependent on the composition of the supporting electrolyte.

In this study ammonia buffer (0.01 M, pH 10) was found to be a suitable medium for the individual detection of cobalt by DPASV. Ammonia buffer solutions containing known amounts of cobalt, ranging from 25 μg/L to 125 μg/L, were used to generated a linear external calibration curve for the detection of cobalt. The calibration experiments were repeated several times and each time the linear calibration curve was determined to be significant based on the F test, coefficient of determination and residual plots. It is therefore considered appropriate to use a linear external calibration curve for the detection of cobalt in ammonia buffer by DPASV with a gold working electrode at the given concentration range.

The calibration experiments were also performed for the detection of nickel in ammonia buffer by DPASV at the gold working electrode. As for the detection of cobalt in ammonia buffer it was considered appropriate to use a linear external calibration curve for the detection of nickel in ammonia buffer, based on statistical the calculations. However, the linear dynamic range of the method only ranges from 25 μg/L nickel to 75 μg/L nickel.

The use of subtractive differential pulse anodic stripping voltammetry (SDPASV) did not improve the significance of the linear calibration curves, nor the symmetry and definition of the analyte peaks, for detection of either nickel and cobalt in ammonia buffer compared to the DPASV. Thus, the use of SDPASV was regarded as unnecessary, especially since it involves the performance of an additional scan for each analysis of a sample.

The simultaneous detection of nickel and cobalt in pure ammonia buffer was not achieved

in this study. The use of complexing agents to separate the joint cobalt and nickel peak that is observed when DPASV is used to analyse a ammonia buffer solution containing both nickel an cobalt was investigated. Of the five complexing agents that were tested, glycine and EDTA were found to be effective. EDTA could be used to mask nickel in solution, thus allowing detection of cobalt alone. Glycine partially separated the joint nickel and cobalt peak. By combining the use of glycine and SDPASV the peaks were almost completely separated. However, care must be taken to ensure that accumulation of deposited cobalt and nickel on the electrode does not interfere with the results.

It was decided in conjunction with the research and development group at Glencore Nikkelverk that joint detection of nickel and cobalt should be applied in the DPASV analyses of their waste water. Activation of the electrode was found to be important in order to get reproducible results. Hypothesis testing was used to help determine if the observed variations in peak height between repetitive analyses of the same waste water samples could be a result of random error or not. Several repetitive analyses of the different waste water samples from the nickel refinery were carried out. In some of the cases the variations in peak height between two parallel analyses of one sample were too large for them to be explained by random error according to the hypothesis test. It is thought that more frequent activation of the gold electrode could increase the reproducibility of the results.

After storage of the gold electrode in rinsed water over night and scanning the electrode from -0.9 V to 0.4 V in waste water diluted with ammonia buffer, the sensitivity towards nickel and cobalt in solution was unexpectedly increased. It is thought that the increased sensitivity is due to a change in the electrode-electrolyte interface, as a result of the storage of the electrode in rinsed water and background scanning, that is similar to the change in electrode-electrolyte interface that occurs when the activation procedure is applied.

A standard addition calibration curve for the detection of nickel by differential pulse anodic stripping voltammetry in a waste water sample from the nickel refinery was generated. Analyses of the waste water samples at the laboratory at Glencore Nikkelverk showed that the cobalt concentration in the waste water is negligible compared to the nickel concentrations. Thus, the standard calibration curve was generated by addition of nickel standard solution to the waste water sample only.

The linear standard addition calibration curve was determined to be significant based on the F test, coefficient of determination and residual plots. Thus, it is appropriate to assume that there is a linear relationship between the measured response and the concentration of

nickel in the sample.

The standard addition curve was used to estimate the nickel concentration in the diluted waste water sample. It was determined to be 0.21 mg/L ± 0.012 mg/L. A deviation of 0.03 mg/L or 15 % from the nickel concentration that was reported as the result of the analysis of the same waste water sample at the laboratory department at the nickel refinery. The elevated result from the DPASV measurements is thought to partly be because the DPASV method in reality measures the combined nickel and cobalt concentration in the waste water, while Glencore Nikkelverk measures the two metals separately. However, since nothing is known about the uncertainty associated with the result provided by Glencore Nikkelverk it is hard compare the two results further.

Although nickel and cobalt have been successfully determined in both synthetic solutions and waste water from the nickel refiner, additional work needs to be done before the DPASV analysis method is put into practice at the nickel refinery. The activation procedure itself, and the needed frequency of application of the activation procedure, should be refined to ensure stability and reproducibility of the method. The long term stability of the method, maintenance procedures and the frequency of maintenance of the voltammetric equipment (including electrodes) must be determined

The pH of the waste water is approximately eight. To reduce the amount of chemicals needed to carry out the DPASV analysis, experiments to see if detection of nickel and cobalt by DPASV can be done directly in the waste water (without ammonia buffer) could be carried out.

References

[1] "River basin management plans. Report on the implementation of the water framework directive," European Commission, 2000. [Online]. Available: http://ec.europa.eu/environment/water/water-framework/pdf/COM-2012-670_EN.pdf

[2] "World summit on sustainable development. Plan of implementation," The United Nations Conference on Environment and Development, 2002. [Online]. Available: http://www.johannesburgsummit.org/html/documents/summit_docs/plan_final1009.doc

[3] Øyvind Mikkelsen, K. Strasunskiene, S. Skogvold, K. H. Schrøder, C. C. Johnsen, M. Rydningen, P. Jonsson, and A. Jonssonc, "Automatic voltammetric system for continuous trace metal monitoring in various environmental samples," *Electroanalysis*, vol. 19, pp. 2085–2092, 2007.

[4] C. Gonzalez, S. Spinelli, J. Gille, E. Touraud, and E. Prichard, "Validation procedure for existing and emerging screening methods," *Trends in Analytical Chemistry*, vol. 26, pp. 315–322, 2007.

[5] S. Saracoglu, M. Soylak, and L. Elci, "Separation/preconcentration of trace heavy metals in urine,sediment and dialysis concentrates by coprecipitation with samarium hydroxide for atomic absorption spectrometry," *Talanta*, vol. 59, pp. 287–293, 2002.

[6] J. Chen and K. C. Teo, "Determination of cadmium, copper, lead and zinc in water samples by flame atomic absorption spectrometry after cloud point extraction," *Analytical Chimica Acta*, vol. 450, pp. 215–222, 2001.

[7] M. Jimoh, W. Frenzel, V. Muller, H. Stephanowitz, and E. Hoffmann, "Development of a hyphenated microanalytical system for the investigation of leaching kinetics of heavy metals in environmental samples," *Analytical Chemistry*, vol. 76, no. 4, pp. 1197–1203, 2004.

[8] A. Ulrich, C. Moor, H. Vonmont, H.-R. Jordi, and M. Lory, "ICP–MS trace-element analysis as a forensic tool," *Analytical and Bioanalytical Chemistry*, vol. 378, pp. 1059–1068, 2003.

[9] Øyvind Mikkelsen, S. M. Skogvold, and K. H. Schrøder, "Continouos heavy metal monitoring systems for application in river and seawater," *Electroanalysis*, vol. 17, pp. 431–439, 2004.

[10] D. R. Crow, *Principles and Applications of Electrochemistry*, 4th ed.   Blackie Academic and Professional, 1994.

[11] J. Golimowski and E. Najdeker, "Voltammetric determination of nickel and palladium in plating baths," *Fresenius Journal of Analytical Chemistry*, vol. 339, pp. 868–870, 1991.

[12] J. J. Lingane and H. Kerlinger, "Polarographic determination of nickel and cobalt. simultaneous determination in presence of iron, copper, chromium, and manganese, and determination of small amounts of nickel in cobalt compounds," *Industrial and Engineering Chemistry*, vol. 13, pp. 77–80, 1941.

[13] M. Morfobos, A. Economou, and A. Voulgaropoulos, "Simultaneous determination of nickel(ii) and cobalt(ii) by square wave adsorptive stripping voltammetry on a rotating-disc bismuth-film electrode," *Analytical Chimica Acta*.

[14] H. Zhang, R. Wollast, J.-C. Vire, and G. J. Patriarche, "Simultaneous determination of cobalt and nickel in sea water by adsorptive cathodic stripping square-wave voltammetry," *Analyst*, vol. 114, pp. 1597–1602, 1989.

[15] D. Sancho, L. Debán, I. Campos, R. Pardo, and M. Vega, "Determination of nickel and cobalt in refined beet sugar by adsorptive cathodic stripping voltammetry without sample pretreatment," *Food Chemistry*.

[16] Øyvind Mikkelsen, S. M. Skogvold, K. H. Schrøder, T. A. Aarhaug, and M. I. Gjerde, "Evaluation of solid electrodes for use in voltammetric monitoring of heavy metals in samples from metallurgic nickel industry," *Analytical and Bioanalytical Chemistry*, vol. 377, pp. 322–326, 2003.

[17] S. Zumdahl, *Chmical Principles*, 7th ed.   Thomson Brooks/Cole, 2007.

[18] D. T. Sawyer, A. Sobkowiak, and J. L. Roberts, Jr., *Electrochemistry for Chemists*, 2nd ed.   John Wiley and Sons, Inc., 1995.

[19] J. Wang, *Analytical Electrochemistry*, 3rd ed.   John Wiley and Sons, Inc., 2000.

[20] D. A. Skoog, D. M. West, F. J. Holler, and S. Crouch, *Fundamentals of Analytical Chemistry*, 8th ed.   Thompson Brooks/Cole.

[21] J. Koryta, J. Dvorak, and L. Kavan, *Principles of Electrochemistry*, 2nd ed.   John Wiley and Sons Ltd., 1993.

[22] P. C. Hiemenz and R. Rajagopalan, *Principles of Collois and Surface Chemistry*, 3rd ed. CRC Press. Taylor & Francis Group, 1997.

[23] J. O. Bockris and S. U. M. Khan, *Surface Electrochemistry. A molecular Level Approach*. Plenum Press, 1993.

[24] J. Wang, *Stripping Analysis. Principles, Instrumentation, and Application*, 1st ed. VCH Publishers, Inc., 1985.

[25] Y. Bonfil, M. Brand, and E. Kirowa-Eisner, "Determination of sub-μg concentrations of copper by anodic stripping voltammetry at the gold electrode," *Analytica Chimica Acta*, vol. 387, pp. 85–95, 1999.

[26] ——, "Characteristics of subtractive anodic stripping voltammetry of pb and cd at silver and gold electrodes," *Analytica Chimica Acta*, vol. 464, pp. 99–114, 2002.

[27] ——, "Trace determination of mercury by anodic stripping voltammetry at the rotating gold electrode," *Analytica Chimica Acta*, vol. 424, pp. 65–76, 2000.

[28] M. F. Toney, J. N. Howard, J. Richer, G. L. Borges, J. G. Gordon, O. R. Mel, D. Yee, and L. B. Sorensen, "Electrochemical deposition of copper on a gold electrode in sulfuric acid: Resolution of the interfacial structure," *Physical Review Letters*.

[29] M. Lovric, "Stripping voltammetry," in *Electroanalytical Methods*, F. Scholz, Ed. Springer, 2005.

[30] Y. Bonfil and E. Kirowa-Eisner, "Determination of nanomolar concentrations of lead and cadmium by anodic-stripping voltammetry at the silver electrode," *Analytica Chimica Acta*, vol. 457, pp. 285–296, 2002.

[31] S. M. Skogvold, "Development and properties of nontoxic solid electrodes for environmental surveillance application in automatic on site determination of metals in natural water and industrial solutions," Ph.D. dissertation, Norwegian University of Science and Technology.

[32] M. M. E. M. Agnese Giacomino, Ornella Abollino, "Parameters affecting the determination of mercury by anodic stripping voltammetry using a gold electrode," *Talanta*.

[33] D. C. Johnson and W. R. LaCourse, "Liquid chromatography with pulsed electrochemical detection at gold and platinum electrodes," *Analytical Chemistry*.

[34] D. D.Perrin, *Masking and Demasking of Chemical Reactions. Theoretical aspects and Practical Applications*, 1st ed. Wiley-Interscience, 1970.

[35] M. M. A. Romia, H. Matsuda, and K. Tokuda, "Polarographic study on the electrode kinetics of the cobalt(ii)-glycine complexes," *Electroanalytical Chemistry and Interfacial Electrochemistry.*

[36] B. E. Conway and J. O. Bockris, "Electrolytic hydrogen evolution kinetics and its relation to the electronic and adsorptive properties of the metal," *Journal of Chemical Physics*, vol. 26, pp. 532–541, 1957.

[37] R. Parsons, "The rate of electrolytic hydrogen evolution and the heath of adsorption of hydrogen," *Transactions of the Faraday Society*, vol. 54, pp. 1053–1063, 1958.

[38] S. Trasatti, "Work function, electronegativity, and electrochemical behaviour of metals III. Electrolytic hydrogen evolution in acid solutions," *Journal of Electroanalytical Chemistry*, vol. 39, pp. 163–184, 1972.

[39] B. E. Conway, "Electrochemical processes involving H adsorbed at metal electrode surfaces," in *Interfacial Electrochemistry. Theory, Experiment, and Applications*, A. Wieckowski, Ed. Marcel Dekker, Inc, 1999.

[40] J. K. Nørskov, T. Bligaard, A. Logadottir, J. R. Kitchin, J. G. Chen, S. Pandelov, and U. Stimmingc, "Trends in the exchange current for hydrogen evolution," *Journal of The Electrochemical Society*, vol. 152, pp. 23–26, 2005.

[41] H. S. Fogler, *Elements of Chemical Reaction Engineering*, 4th ed. Pearson Education, 2006.

[42] L. I. Krishtalik, "Hydrogen overvoltage and adsorption phenomena: Part III. Effect of the adsorption energy of hydrogen on overvoltage and the mechanism of the cathodic process," in *Advances in Electrochemistry and Electrochemical Engineering*, P. Delahay, Ed. Interscience, 1970, vol. 7.

[43] M. A. V. Devanathan and B. V. K. S. R. A. Tilak, "On the specific adsorption of anions in the electrical double layer," *Proceedings of the Royal Society of London. Series A, Mathematical and Physical*, vol. 290, pp. 527–546, 1966.

[44] P. V. Popat and N. Hackerman, "Capacity of the electrical double layer and adsorption at the polarized platinum electrodes. I. Adsorption of anions," *Journal of Physical Chemistry*, vol. 62, pp. 1198–1203, 1958.

[45] G. Valette, A. Hamelin, and R. Parsons, "Specific adsorption on silver single crystals in aqueous solutions," *Zeitschrift für Physikalische Chemie Neue Folge,*, vol. 113, pp. 71–89, 1978.

[46] T. Greibrokk, E. Lundanes, and K. E. Rasmussen, *Kromatografi. Separasjon og deteksjon.*, 3rd ed. Universitetsforlaget, 1994.

[47] J. N. Miller, "Basic statistical methods for analytical chemistry part 2. calibration and regression methods. a review," *Analyst.*

[48] K. H. Esbensen, *Multivariate Data Analysis - in practice*, 5th ed. CAMO, 2001.

[49] D. C. Montgomery, *Introduction to Statistical Quality Control*, 5th ed. John Wiley & Sons Inc., 2005.

[50] G. G. Hammes and J. I. Steinfeld, "Relaxation spectra of some nickel (ii) and cobalt (ii) complexes," *Journal of the American Chemistry Society.*

A   Statistical calculations

In this appendix calculations associated with the hypothesis tests that have been carried out and the calibration curves that have been generated in this study, is presented. Residual plots for the linear calibration curves generated by the least squares method are also given here.

A.1   External standard calibration curves for the detection of nickel in ammonia buffer

Figures 33, 35 and 37 show the calculated statistical properties associated with the each of the three standard calibration curves (see Figure 12) for detection of nickel in ammonia buffer by DPASV that have been generated by the least squares method. Figures 34, 36 and 38 show the residual plots corresponding to the calculations in Figures 33, 35 and 37, respectively. The Equations that have been used to calculate these properties are given in section 2.6.2.

Calibration curve by the least squares method

	Peak height [uA]	Concentration [ug/L]
	1,80	25,00
	2,73	50,00
	3,53	75,00
Mean	2,686666667	50
Number of observations, N	3	3
SSxx		1250
SSyy	1,499266667	
SSxy	43,25	
m	0,0346	
b	0,956666667	
sr	0,053072278	
sm	0,001501111	
sb	0,081069243	
SSresid	0,002816667	
Number of degrees of freedom SSresid, df_{resid}	1	
SSregr	1,49645	
Number of degrees of freedom SSregr, df_{regr}	1	
Significance level, α	0,05	
F	531,2840237	
Critical F value	161,45	

Figure 33: Calibration curve statistics for the exsternal standard calibration curve for the determination of nickel in ammonia buffer by DPASV shown in Figure 12 with equation y = 0.0346x + 0,9567.
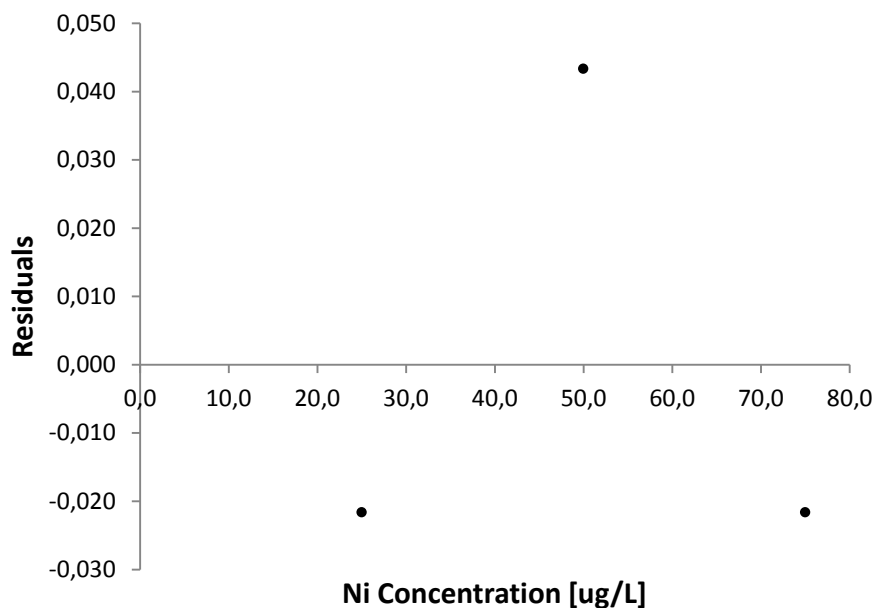
I

Figure 34: Residual plot from the least squares method used to generate the standard addtion calibration curve showin in Figure 12 with equation y = 0.0346x + 0,9567.

A.2 External standard calibration curves for the detection of cobalt in ammonia buffer

Figures 39, 41 and 43 show the calculated statistical properties associated with the each of the three standard calibration curves (see Figure 15) for detection of cobalt in ammonia buffer by DPASV that have been generated by the least squares method. Figures 40, 42 and 44 show the residual plots corresponding to the calculations in Figures 39, 41 and 43, respectively. The Equations that have been used to calculate these properties are given in section 2.6.2.

A.3 Standard addition calibration curve statis

Figure 45 shows the calculated statistical properties associated with the standard calibration curve for detection of nickel in waste water samples by DPASV that has been generated in this study. The Equations that have been used in the calculations are given in section 2.6.2. The residual plot is displayed in Figure 46.

Calibration curve by the least squares method

	Peak height [uA]	Concentration [ug/L]
	1,20	25,00
	2,13	50,00
	3,01	75,00
Mean	2,113333333	50
Number of observations, N	3	3
SSxx		1250
SSyy	1,638466667	
SSxy	45,25	
m	0,0362	
b	0,303333333	
sr	0,020412415	
sm	0,00057735	
sb	0,031180478	
SSresid	0,000416667	
Number of degrees of freedom SSresid, df_{resid}	1	
SSregr	1,63805	
Number of degrees of freedom SSregr, df_{regr}	1	
Significance level, α	0,05	
F	3931,32	
Critical F value	161,45	

Figure 35: Calibration curve statistics for the exsternal standard calibration curve for the determination of nickel in ammonia buffer by DPASV shown in Figure 12 with equation y = 0.0362x + 0,3033.
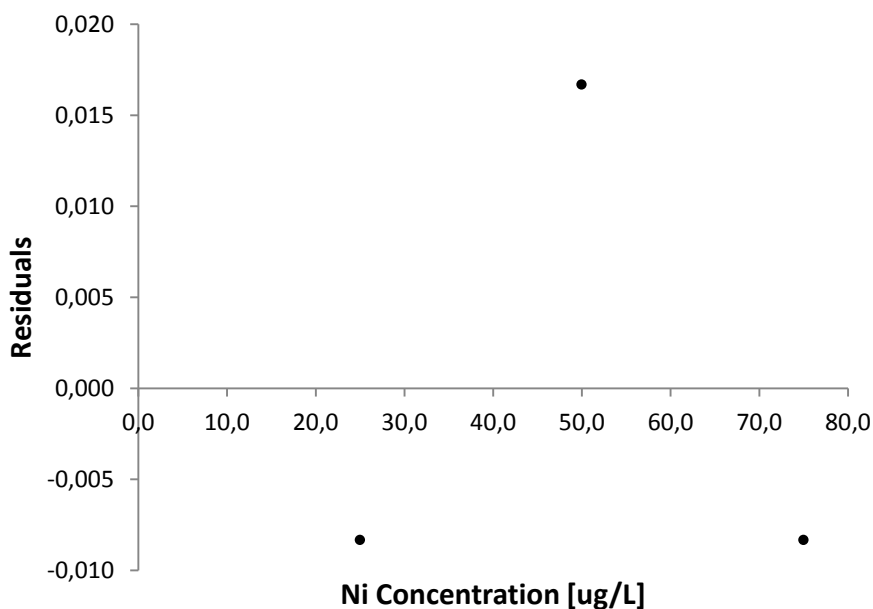

Figure 36: Residual plot from the least squares method used to generate the standard addtion calibration curve showin in Figure 12 with equation y = 0.0362x + 0,3033.

Calibration curve by the least squares method

	Peak height [uA]	Concentration [ug/L]
	1,43	25,00
	2,30	50,00
	3,32	75,00
Mean	2,35	50
Number of observations, N	3	3
SSxx		1250
SSyy	1,7898	
SSxy	47,25	
m	0,0378	
b	0,46	
sr	0,061237244	
sm	0,001732051	
sb	0,093541435	
SSresid	0,00375	
Number of degrees of freedom SSresid, df_{resid}	1	
SSregr	1,78605	
Number of degrees of freedom SSregr, df_{regr}	1	
Significance level, α	0,05	
F	476,28	
Critical F value	161,45	

Figure 37: Calibration curve statistics for the exsternal standard calibration curve for the determination of nickel in ammonia buffer by DPASV shown in Figure 12 with equation y = 0.0378x + 0,46.
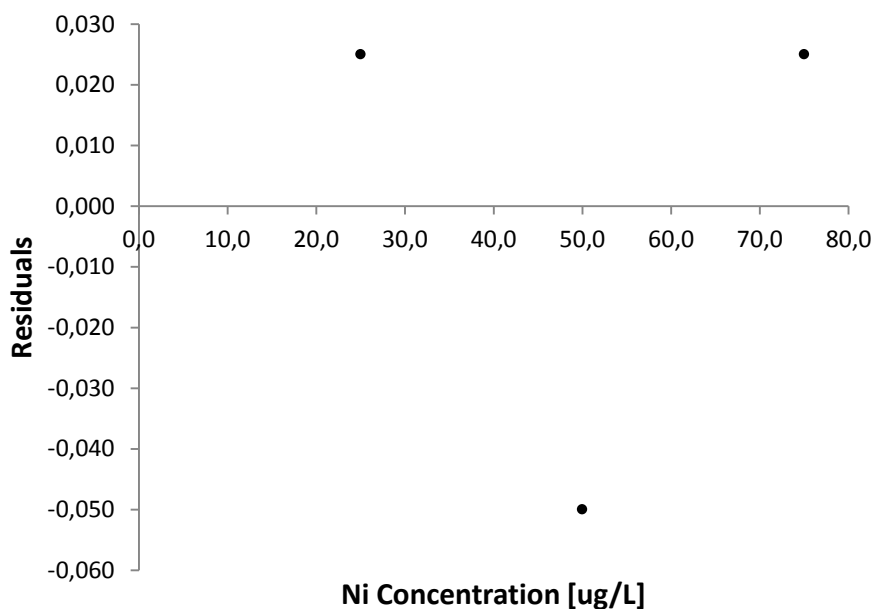

Figure 38: Residual plot from the least squares method used to generate the standard addtion calibration curve showin in Figure 12 with equation y = 0.0378x + 0,46.

Calibration curve by the least squares method

	Peak height [uA]	Concentration [ug/L]
	1,27	25,00
	2,17	50,00
	3,28	75,00
	4,24	100,00
	5,22	125,00
Mean	3,236	75
Number of observations, N	5	5
SSxx		6250
SSyy	9,94772	
SSxy	249,25	
m	0,03988	
b	0,245	
sr	0,050431472	
sm	0,000637913	
sb	0,022570836	
SSresid	0,00763	
Number of degrees of freedom SSresid, df_{resid}	3	
SSregr	9,94009	
Number of degrees of freedom SSregr, df_{regr}	1	
Significance level, α	0,05	
F	3908,292267	
Critical F value	10,13	

Figure 39: Calibration curve statistics for the exsternal standard calibration curve for the determination of nickel in ammonia buffer by DPASV shown in Figure 12 with equation y = 0.0346x + 0,9567.
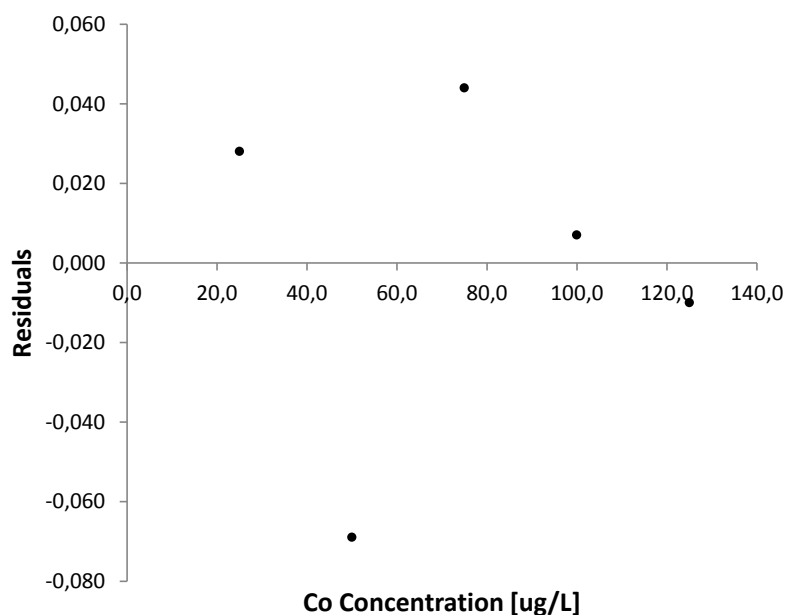

Figure 40: Residual plot from the least squares method used to generate the standard addtion calibration curve showin in Figure 12 with equation y = 0.0346x + 0,9567.

Calibration curve by the least squares method

	Peak height [uA]	Concentration [ug/L]
	1,15	25,00
	1,85	50,00
	2,90	75,00
	3,82	100,00
	4,58	125,00
Mean	2,86	75
Number of observations, N	5	5
SSxx		6250
SSyy	7,8258	
SSxy	220,75	
m	0,03532	
b	0,211	
sr	0,098166525	
sm	0,001241719	
sb	0,043927544	
SSresid	0,02891	
Number of degrees of freedom SSresid, df_{resid}	3	
SSregr	7,79689	
Number of degrees of freedom SSregr, df_{regr}	1	
Significance level, α	0,05	
F	809,0857835	
Critical F value	10,13	

Figure 41: Calibration curve statistics for the exsternal standard calibration curve for the determination of nickel in ammonia buffer by DPASV shown in Figure 12 with equation y = 0.0362x + 0,3033.
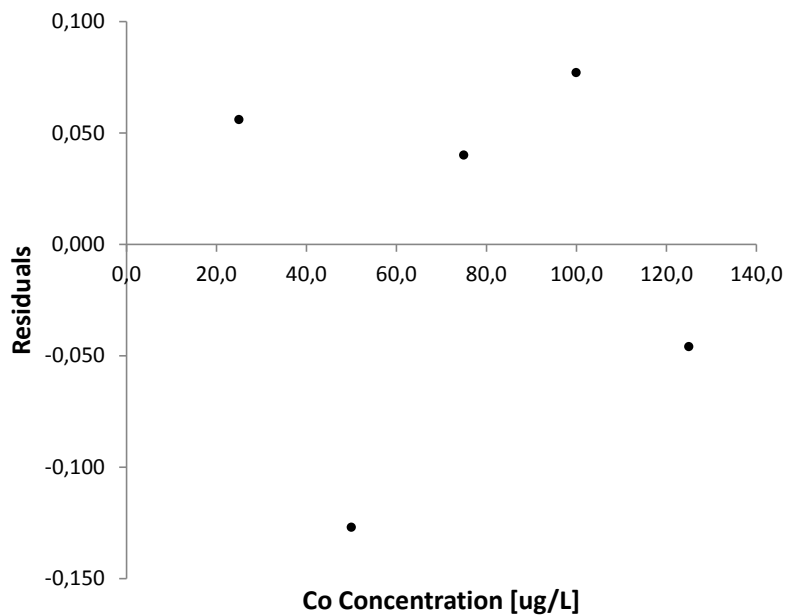

Figure 42: Residual plot from the least squares method used to generate the standard addtion calibration curve showin in Figure 12 with equation y = 0.0362x + 0,3033.

Calibration curve by the least squares method

	Peak height [uA]	Concentration [ug/L]
	1,27	25,00
	2,17	50,00
	3,28	75,00
	4,24	100,00
	5,22	125,00
Mean	3,236	75
Number of observations, N	5	5
SSxx		6250
SSyy	9,94772	
SSxy	249,25	
m	0,03988	
b	0,245	
sr	0,050431472	
sm	0,000637913	
sb	0,022570836	
SSresid	0,00763	
Number of degrees of freedom SSresid, df_{resid}	3	
SSregr	9,94009	
Number of degrees of freedom SSregr, df_{regr}	1	
Significance level, α	0,05	
F	3908,292267	
Critical F value	10,13	

Figure 43: Calibration curve statistics for the exsternal standard calibration curve for the determination of nickel in ammonia buffer by DPASV shown in Figure 12 with equation y = 0.0378x + 0,46.
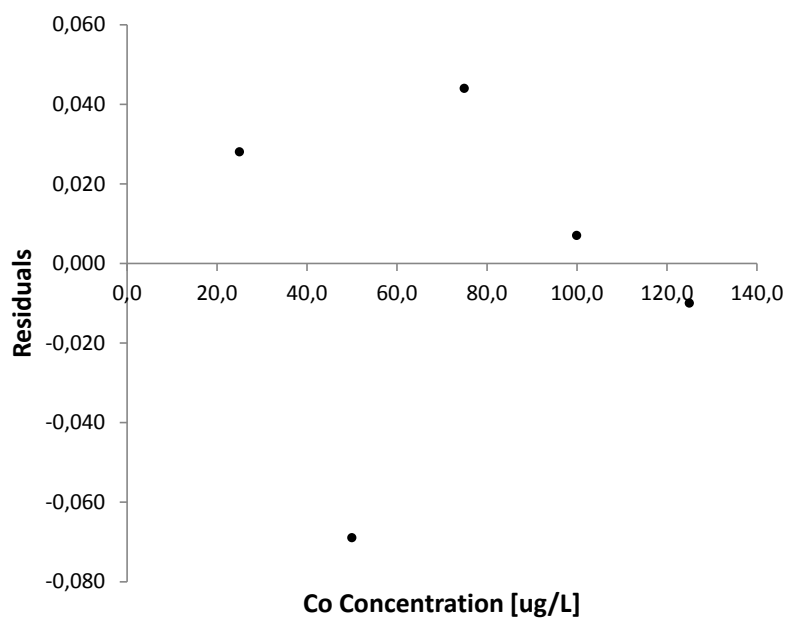

Figure 44: Residual plot from the least squares method used to generate the standard addtion calibration curve showin in Figure 12 with equation y = 0.0378x + 0,46.

Calibration curve by the least squares method

	Peak height [uA]	Concentration [mg/L]
	2,478581	0
	8,566455	0,1
	14,86093	0,2
	20,66942	0,3
Mean	11,6438465	0,15
Number of observations, N	4	4
SSxx		0,05
SSyy	185,2830334	
SSxy	3,0433496	
m	60,866992	
b	2,5137977	
sr	0,147474783	
sm	0,659527279	
sb	0,123386256	
sc	0,002400891	
SSresid	0,043497623	
Number of degrees of freedom SSresid, df_{resid}	2	
SSregr	185,2395358	
Number of degrees of freedom SSregr, df_{regr}	1	
Significance level, α	0,05	
F	8517,225631	
Critical F value	18,51	

Figure 45: Calibration curve statistics for the standard addition calibration curve for the determination of nickel in waste water samples.
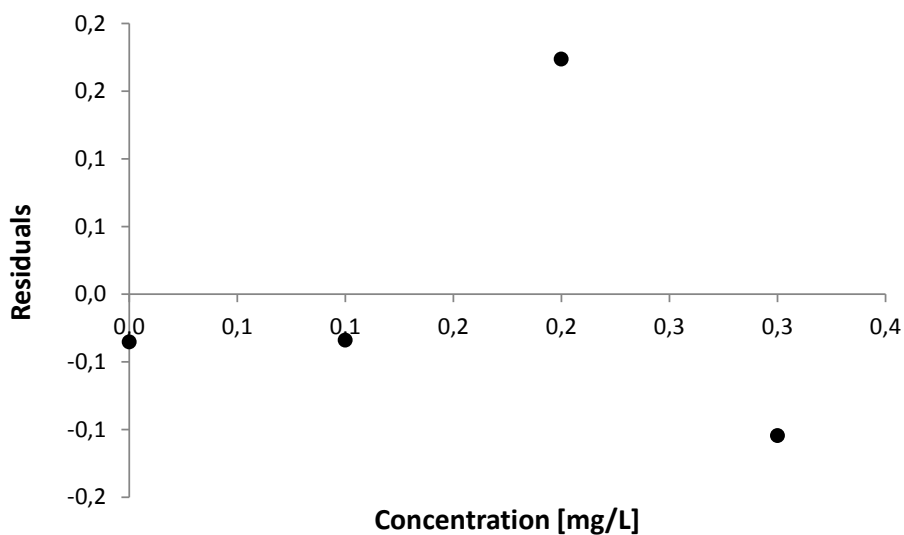

Figure 46: Residual plot from the least squares method used to generate the standard addtion calibration curve showin in Figure 32

B   Hypothesis test

In this appendix the calculations associated with the hypothesis test that have been carried out in this study are shown.

Figure 47 shows the calculations of the hypothesis test carried out on the results from the analysis of a the waste water sample as shown Figure 23. The data was divided into two sets and the two experimental means was compared by a hypothesis test.

t-Test: Two-Sample Assuming Equal Variances

	Variable 1	Variable 2
	2,086171	2,164924
	2,036708	2,164924
	2,272181	2,164924
Mean	2,131686667	2,164924
Number of observations	3	3
Pooled Variance, s_{pooled}	0,087794192	
Number of degrees of freedom	4	
t value	0,463666816	
Significance level, α	0,3	
P value	0,666994131	
Critical t value	1,134	

Figure 47: Hypothesis test on the the results from the analysis of the waste water sample as shown Figure 23. Variable 1 and variable 2 are the peak heights of the joint cobalt and nickel peaks, obtained from Figure 23, in each set of data.

Figure 48 shows the calculations of the hypothesis test carried out on the results from the two repetitive analyses of a the waste water sample of nickel concentration 0.47 mg/L as shown Figures 28 and 29. The two experimental means of the two data sets were compared by a hypothesis test.

Figure 49 shows the calculations of the hypothesis test carried out on the results from the two repetitive analyses of a the waste water sample of nickel concentration 0.36 mg/L as shown Figures 28 and 29. The two experimental means of the two data sets were compared by a hypothesis test.

Figure 50 shows the calculations of the hypothesis test carried out on the results from the two repetitive analyses of a the waste water sample of nickel concentration 0.25 mg/L as shown Figures 28 and 29. The two experimental means of the two data sets were compared by a hypothesis test.

Figure 50 shows the calculations of the hypothesis test carried out on the results from the two repetitive analyses of a the waste water sample of nickel concentration 0.20 mg/L as

t-Test: Two-Sample Assuming Equal Variances

	Variable 1	Variable 2
	5,59	4,897134
	5,476875	5,215765
	5,510625	5,439388
	5,593125	5,437162
Mean	5,54265625	5,24736225
Number of observations, N	4	4
Pooled Variance, s_{pooled}	0,1856061	
Number of degrees of freedom	6	
t value	2,249973355	
Significance level, α	0,05	
P value	0,065443599	
Critical t value	2,447	

Figure 48: Hypothesis test on the results from the two repetitive analyses of the waste water sample of nickel concentration 0.47 mg/L as shown Figures 28 and 29. Variable 1 and variable 2 are the peak heights of the joint cobalt and nickel peaks, obtained from Figures 28 and 29, in each set of data.

shown Figures 28 and 29. The two experimental means of the two data sets were compared by a hypothesis test.

t-Test: Two-Sample Assuming Equal Variances

	Variable 1	Variable 2
	4,540625	4,415765
	4,26875	4,27625
	4,29875	4,116875
	4,2	3,871875
Mean	4,32703125	4,17019125
Number of observations, N	4	4
Pooled Variance, s_{pooled}	0,195510398	
Number of degrees of freedom	6	
t value	1,134493395	
Significance level, α	0,05	
P value	0,299869522	
Critical t value	2,447	

Figure 49: Hypothesis test on the results from the two repetitive analyses of the waste water sample of nickel concentration 0.36 mg/L as shown Figures 28 and 29. Variable 1 and variable 2 are the peak heights of the joint cobalt and nickel peaks, obtained from Figures 28 and 29, in each set of data.

t-Test: Two-Sample Assuming Equal Variances

	Variable 1	Variable 2
	3,225508	2,989088
	3,208236	2,917627
	3,054559	2,843491
	2,996722	2,665704
Mean	3,12125625	2,8539775
Number of observations, N	4	4
Pooled Variance, s_{pooled}	0,126658458	
Number of degrees of freedom	6	
t value	2,984318917	
Significance level, α	0,05	
P value	0,024499432	
Critical t value	2,447	

Figure 50: Hypothesis test on the results from the two repetitive analyses of the waste water sample of nickel concentration 0.25 mg/L as shown Figures 28 and 29. Variable 1 and variable 2 are the peak heights of the joint cobalt and nickel peaks, obtained from Figures 28 and 29, in each set of data.

t-Test: Two-Sample Assuming Equal Variances

|	Variable 1	Variable 2
	2,28875	2,50875
	2,59875	2,40375
	2,624375	2,31375
Mean	2,503958333	2,40875
Number of observations, N	3	3
Pooled Variance, s_{pooled}	0,149038804	
Number of degrees of freedom	4	
t value	0,782386297	
Significance level, α	0,05	
P value	0,477711533	
Critical t value	2,447	

Figure 51: Hypothesis test on the results from the two repetitive analyses of the waste water sample of nickel concentration 0.20 mg/L as shown Figures 28 and 29. Variable 1 and variable 2 are the peak heights of the joint cobalt and nickel peaks, obtained from Figures 28 and 29, in each set of data.

C   Detection of nickel and cobalt in ammonia buffer

The figures in this appendix display the voltammograms from the detection of nickel and cobalt in ammonia buffer by differential pulse anodic stripping voltammetry (DPASV) and subtractive differential pulse anodic stripping voltammetry (SDPASV). Figures 52 and 54 display two repetitive detections of nickel in ammonia buffer by DPASV and SDPASV, and Figured 56, and 58 display two repetitive detections of cobalt in ammonia buffer by DPASV and SDPASV.

Figures 53 and 55 show the external standard calibration curve corresponding to the DPASV and SDPASV measurements of nickel in ammonia buffer displayed in Figures 52 and 54, respectively. Figures 57 and 59 show the external standard calibration curve corresponding to the DPASV and SDPASV measurements of nickel in ammonia buffer displayed in Figures 56 and 58, respectively.
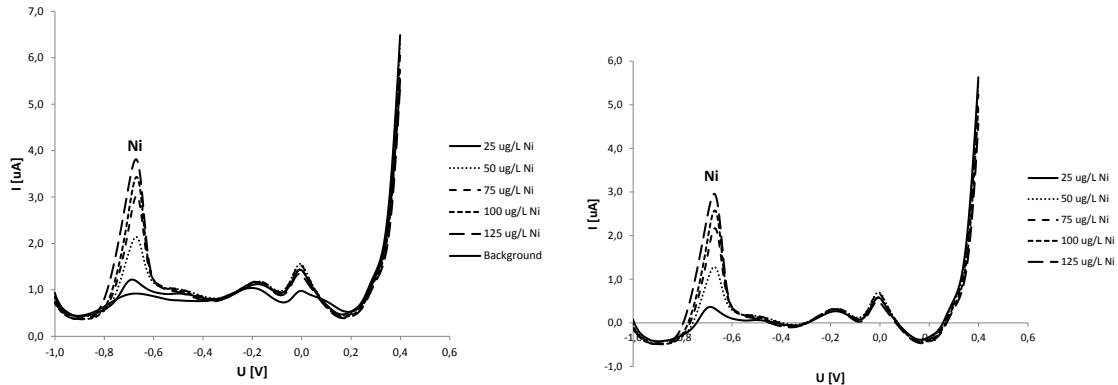
(a) Differnetial pulse anodic stripping voltamme-try

(b) Subtractive differential pulse anodic strip-ping voltammetry

Figure 52: Detection of nickel(II) in ammonia buffer (0.01 M, pH 10) by differential pulse anodic stripping voltammetry and subtractive differential pulse anodic stripping voltammetry. Scan rate 15 mV/s, pulse amplitude 50 mV, deposition potential - 1.2 V, deposition time 30 seconds, scan from -1.0 V to 0.4 V. Nickel standard solution (30 mg/L) has been successively added, 25 μ L at the time, to the ammonia buffer to create sample solutions of known nickel concentration. The nickel concentration ranges from 25 μg/L to 125 μg/L as indicated in the figure.
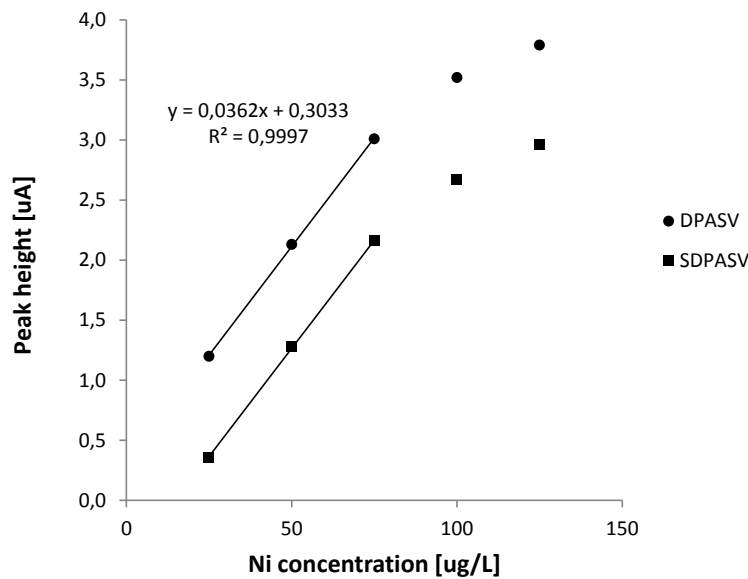

Figure 53: External standard calibration curve corresponding to the solutions analysed by differential puøse anodic stripping voltammetry and subtractive anodic stripping voltammetry as displayed in Figure 52. The linear dynamic range for detection of nickel in ammonia buffer ends at about 75 μg/L nickel, thus the correlation curve is conctructed using the three first calibration points (25 μg/L to 75 μg/L). The coefficient of determination (R^2) and the equation of the calibration curves are given in the figure.
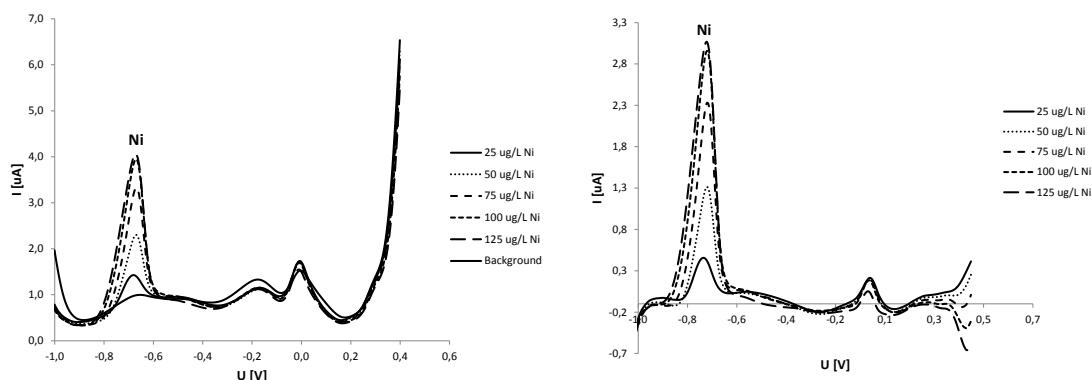
(a) Differnetial pulse anodic stripping voltamme- (b) Subtractive differential pulse anodic strip-
try   ping voltammetry

Figure 54: Detection of nickel(II) in ammonia buffer (0.01 M, pH 10) by differential pulse anodic stripping voltammetry and subtractive differential pulse anodic stripping voltammetry. Scan rate 15 mV/s, pulse amplitude 50 mV, deposition potential - 1.2 V, deposition time 30 seconds, scan from -1.0 V to 0.4 V. Nickel standard solution (30 mg/L) has been successively added, 25 μ L at the time, to the ammonia buffer to create sample solutions of known nickel concentration. The nickel concentration ranges from 25 μg/L to 125 μg/L as indicated in the figure.
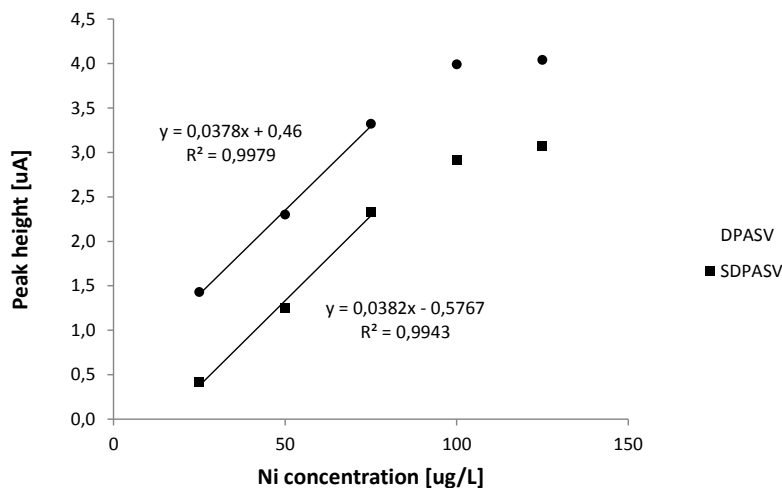

Figure 55: External standard calibration curve corresponding to the solutions analysed by differential puøse anodic stripping voltammetry and subtractive anodic stripping voltammetry as displayed in Figure 54. The linear dynamic range for detection of nickel in ammonia buffer ends at about 75 μg/L nickel, thus the correlation curve is conctructed using the three first calibration points (25 μg/L to 75 μg/L). The coefficient of determination (R^2) and the equation of the calibrations curves are given in the figure.

XV
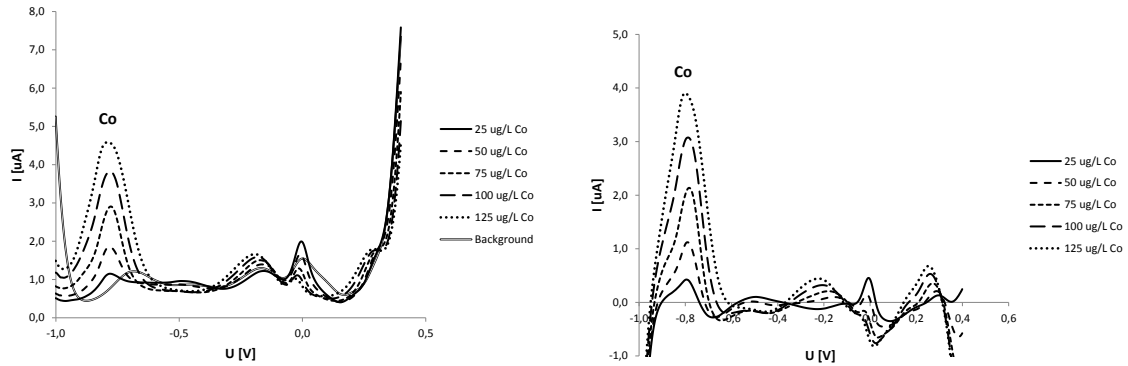
(a) Differnetial pulse anodic stripping voltammetry

(b) Subtractive differential pulse anodic stripping voltammetry

Figure 56: Detection of nickel(II) in ammonia buffer (0.01 M, pH 10) by differential pulse anodic stripping voltammetry and subtractive differential pulse anodic stripping voltammetry. Scan rate 15 mV/s, pulse amplitude 50 mV, deposition potential - 1.2 V, deposition time 30 seconds, scan from -1.0 V to 0.4 V. Nickel standard solution (30 mg/L) has been successively added, 25 μ L at the time, to the ammonia buffer to create sample solutions of known nickel concentration. The nickel concentration ranges from 25 μg/L to 125 μg/L as indicated in the figure.
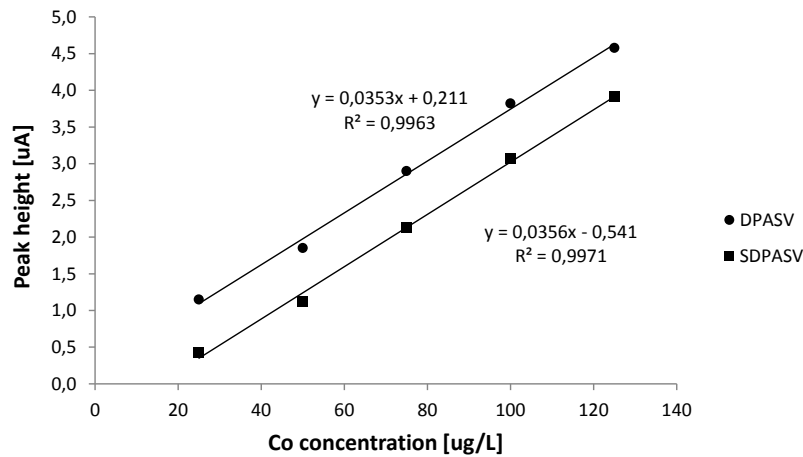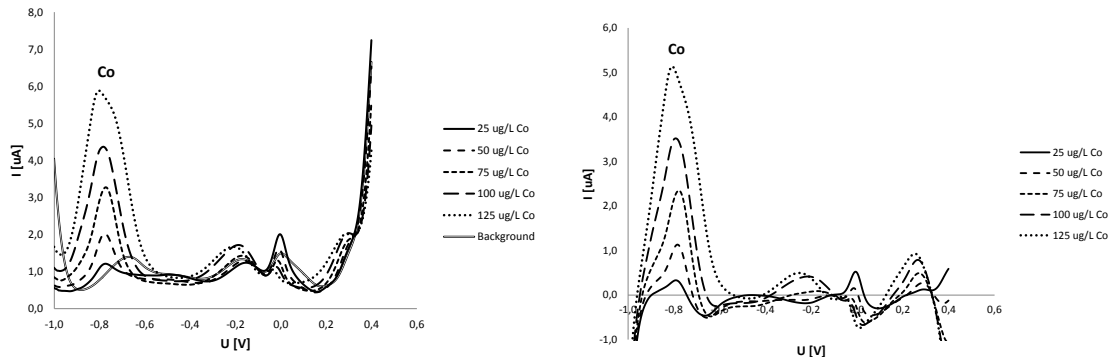

Figure 57: External standard calibration curve corresponding to the solutions analysed by DPASV and SDPASV as displayed in Figure 56. The coefficient of determination (R^2) and the equation of the calibration curves are given in the figure

XVI

(a) Differnetial pulse anodic stripping voltamme-
try

(b) Subtractive differential pulse anodic strip-
ping voltammetry

Figure 58: Detection of nickel(II) in ammonia buffer (0.01 M, pH 10) by differential pulse anodic stripping voltammetry and subtractive differential pulse anodic stripping voltammetry. Scan rate 15 mV/s, pulse amplitude 50 mV, deposition potential - 1.2 V, deposition time 30 seconds, scan from -1.0 V to 0.4 V. Nickel standard solution (30 mg/L) has been successively added, 25 μ L at the time, to the ammonia buffer to create sample solutions of known nickel concentration. The nickel concentration ranges from 25 μg/L to 125 μg/L as indicated in the figure.
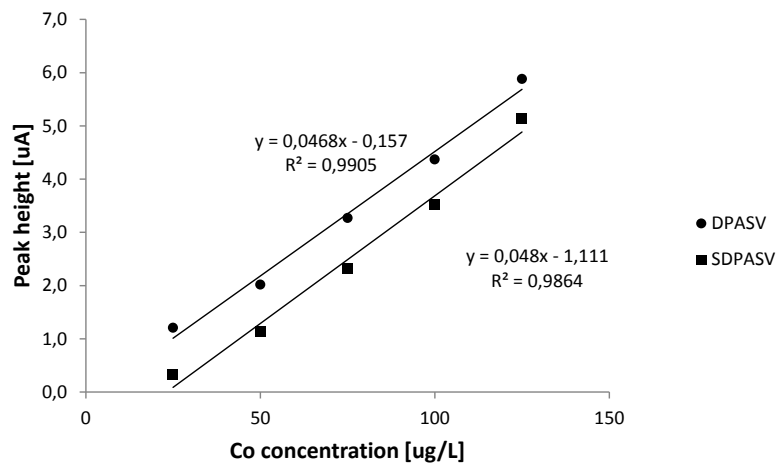

Figure 59: External standard calibration curve corresponding to the solutions analysed by DPASV and SDPASV as displayed in Figure 58. The squared coefficient of determination (R^2) and the equation of the calibration curves are given in the figure

D   Waste water samples from the nickel refinery

In this appendix details about the seven waste water samples that were provided by Glencore Nikkelverk is presented. Figure 60 shows the results of analyses of the nickel and cobalt concentration in the waste water samples that were carried out by the laboratory department at Glencore Nikkelverk. An additional waste water sample that was not analysed at the nickel refiner was also provided.

Utslippsprøver fra Glencore Nikkelverk,

Konserveringsmiddel: 5 ml HCl (kons.) til 250 ml prøve.

	Ni i mg/l	Co i mg/l	Cu i mg/l	Fe i mg/l	Zn i mg/l
06.nov	0,47	0,01	<0,01	<0,01	<0,01
07.nov	0,36	<0,01	<0,01	0,02	<0,01
08.nov	0,18	<0,01	<0,01	0,02	<0,01
Mnd.pr. Aug	0,20	0,01	0,03	0,04	<0,01
Mnd.pr. sep	0,25	0,01	0,02	0,04	<0,01
Mnd.pr.okt	0,16	<0,01	0,02	0,03	<0,01

Figure 60: Results of analyses of the nickel and cobalt concentration in the waste water samples that were carried out by the laboratory department at Glencore Nikkelverk.
.